Physica Scripta

OPEN ACCESS

RECEIVED
20 November 2025

REVISED
2 February 2026

ACCEPTED FOR PUBLICATION
12 February 2026

PUBLISHED
23 February 2026

PAPER

Commutative and non-commutative signatures of anisotropic inflation: constraints from planck PR4 data

Akash Gandhi*

Department of Physics, Indian Institute of Technology, Kalyanpur, Kanpur, 208016, Uttar Pradesh, India

* Author to whom any correspondence should be addressed.

E-mail: gakash@iitk.ac.in

Keywords: anisotropic cosmology, non-commutative geometry, primordial power spectrum, cosmic microwave background

Abstract

We present a comparative study of anisotropic inflationary signatures in both commutative and non-commutative spacetime frameworks, using three anisotropic metrics (Models I–III) as inflationary backgrounds. For each model, we consider the primordial scalar power spectrum computed with the in–in formalism, obtaining the leading real (quadrupolar) modulation from geometric shear and the leading imaginary (dipolar) modulation from spacetime non-commutativity. These spectra are propagated to CMB anisotropies and tested against *Planck* PR4 temperature data (`Commander` NPIPE) via a unified, signal-matched likelihood framework based on complex Bipolar Spherical Harmonic (BipoSH) coefficients, specifically targeting the dipole sector $L = 1$ coupling adjacent multipoles $(\ell, \ell + 1)$. This unified framework ensures methodological consistency in model comparison by defining a common data vector $\hat{\mathbf{D}}$ that encompasses both real-valued (commutative) and imaginary-valued (non-commutative) anisotropic signatures, ensuring mathematically valid Bayesian evidence calculations. We implement a Bayesian pipeline that jointly samples standard ΛCDM parameters and model parameters (initial shear amplitude, orientation, and non-commutative scale), estimating posterior distributions and model evidences on an equal statistical footing. Our analysis yields stringent upper limits on residual inflationary shear $[(\sigma/H) < 1.8 \times 10^{-5}]$ and non-commutative effects $[\alpha < 0.0069 \text{at} 95\% \text{ C.L.}]$, with Bayesian evidence favoring non-commutative models over geometric shear by $\Delta \ln B \approx 3-5$, though both remain disfavored relative to isotropic ΛCDM. We discuss implications for the cosmic no-hair conjecture and prospects for improved tests with future CMB polarization and higher-resolution datasets.

1. Introduction

The standard model of cosmology (ΛCDM), has achieved remarkable success in describing a wide array of cosmological observations, from the large-scale distribution of galaxies to the abundances of light [1]. Its most stringent test comes from the temperature and polarization anisotropies of the Cosmic Microwave Background (CMB), which have been mapped with exquisite precision by the Planck satellite [2]. The statistical properties of the CMB are overwhelmingly consistent with the foundational Cosmological Principle, which posits that the Universe is statistically homogeneous and isotropic on large scales. Despite this success, several large-scale anomalies have persisted in the data, hinting at potential cracks in the standard cosmological paradigm [3]. The most statistically significant and persistent of these is the Hemispherical Power Asymmetry (HPA), first identified in data from the Wilkinson Microwave Anisotropy Probe (WMAP) [4–8] and subsequently confirmed with high significance in multiple Planck data releases, including the most recent Public Release 4 (PR4) [9]. The HPA is phenomenologically well-described by a dipole modulation [10] of the otherwise statistically isotropic CMB temperature field, of the form

$$\Delta T(\mathbf{n}) = \Delta T_{\rm iso}(\mathbf{n})(1 + A\mathbf{p}\cdot\mathbf{n}) \quad (1)$$

where A is the modulation amplitude and $\mathbf{p}$ is a preferred direction on the sky. A crucial characteristic of the HPA is its scale dependence: the asymmetry is prominent at large angular scales (multipoles $\ell \leqslant 64$) but is consistent with zero at smaller scales [11]. This behavior strongly suggests that the HPA is not a late-time systematic or astrophysical effect, but rather has a primordial origin rooted in the physics of cosmic inflation [12, 13].

We investigate two distinct and physically motivated paradigms for generating such a primordial anisotropy during inflation.

1. **Commutative (Geometric) Anisotropy:** This framework posits that the asymmetry is a classical, geometric remnant of a pre-inflationary anisotropic expansion phase. While inflation is exceptionally efficient at smoothing the Universe, the cosmic no-hair conjecture which states that all initial anisotropies are exponentially diluted away may be violated to a small, observable degree [14]. Theoretical models of inflation in anisotropic spacetimes, such as the Bianchi models, generically predict that a residual geometric shear will imprint a real, even-parity (quadrupolar) modulation on the primordial power spectrum [15–19].
2. **Non-Commutative (Quantum-Gravitational) Anisotropy:** This alternative paradigm proposes that the effect stems from new physics at the Planck scale, where spacetime itself may be non-commutative, with spacetime coordinates becoming operators that satisfy the commutation relation $[x^{\mu}, x^{\nu}] = i\theta^{\mu\nu}$. The non-commutativity tensor $\theta^{\mu\nu}$ introduces a fundamental directionality into the fabric of spacetime. This leads to a distinct primordial signature: an imaginary, odd-parity (dipolar) modulation of the power spectrum, representing a violation of parity symmetry [20, 21].

The fundamental mathematical distinction between these two predictions, one producing a real, quadrupolar power spectrum modulation, the other an imaginary, dipolar one is not merely phenomenological. It traces directly to the underlying physics. Geometric shear represents a symmetric stretching and squeezing of spacetime, an inherently even-parity process that naturally sources a quadrupolar ($\ell = 2$) signature [15]. In contrast, spacetime non-commutativity introduces a fundamental vector-like directionality via the θ components, a parity-violating effect that sources a dipolar ($\ell = 1$) signature [22, 23]. This dichotomy implies that the CMB anisotropies contain the necessary information to distinguish between a classical remnant of initial conditions and a quantum signature of new gravitational physics.

Inflation, a phase of accelerated expansion in the very early Universe, provides the most compelling mechanism for generating the primordial curvature perturbations that seed large-scale structure, while simultaneously explaining the observed near-flatness and the causal coherence of the cosmic microwave background (CMB) on super-horizon angular scales [2, 24]. Crucially for the present work, inflation also furnishes a physically well-motivated arena in which small violations of statistical isotropy can arise: residual geometric shear in anisotropic inflationary backgrounds can imprint real, even-parity modulations of the primordial spectrum, whereas Planck-scale new physics such as spacetime non-commutativity can induce distinctive parity-odd (imaginary) dipolar signatures. Because the CMB is a linear probe of these primordial initial conditions, precision measurements—in particular the reduced-noise Planck PR4 (NPIPE) temperature maps—allow us to test such inflationary anisotropy scenarios quantitatively and to constrain both commutative (classical) and non-commutative (quantum-gravitational) departures from ΛCDM within a unified Bayesian framework [20, 25, 26].

The primary objective of this work is to perform the first direct, comparative Bayesian analysis of these two paradigms. We test three physically motivated anisotropic inflationary metrics under both commutative and non-commutative assumptions. Our analysis leverages the latest Planck PR4 (NPIPE) dataset, which is characterized by significantly reduced noise and systematic effects, providing the most robust CMB temperature maps to date for this investigation [27]. The continued presence of the HPA signal in the PR4 data [28] makes this analysis both timely and crucial. By computing the Bayesian evidence for each model, we will provide a quantitative assessment of which physical picture offers a more compelling explanation for the observed large-scale anisotropy in the CMB.

A critical methodological challenge arises when comparing models that predict orthogonal signatures in the harmonic domain. Geometric shear induces real-valued, even-parity (quadrupolar/effective dipolar) correlations between adjacent multipoles, whilst spacetime non-commutativity induces imaginary-valued, odd-parity (dipolar) correlations. To preserve fidelity to these distinct physical mechanisms, we adopt a novel unified likelihood framework based on *complex Bipolar Spherical Harmonic (BipoSH) coefficients*. The BipoSH formalism provides a natural generalization of the isotropic angular power spectrum C_ℓ to include off-diagonal multipole correlations. By extracting BipoSH coefficients $\hat{A}^{LM}_{\ell\ell'}$ from the Planck PR4 data and explicitly treating their real and imaginary parts as distinct sectors of a single data vector $\hat{\mathbf{D}}$, we construct a statistical arena that

Table 1. Anisotropic inflationary background models [29].

Model name	Metric line element (ds^2)	Description of anisotropy evolution
Model I	$dt^2 - 2\sigma dz dt - a^2(t)(dx^2 + dy^2 + dz^2)$	Constant shear in a fixed direction.
Model II	$dt^2 - a^2(t)(dx^2 + dy^2) - b^2(t)dz^2$	Dynamical shear, decays as $\propto a_{\rm avg}^{-3}$.
Model III	Modification of Model II	Transient shear, becomes negligible after ∼1 e-fold.

satisfies the requirement for a consistent data vector whilst maintaining orthogonal sensitivity to real (commutative) and imaginary (non-commutative) anisotropic signals.

2. Primordial power spectra from anisotropic inflation

2.1. Anisotropic background metrics

We consider a spatially flat universe with a background geometry that exhibits a small, direction-dependent expansion rate. We analyze three specific Bianchi I-type metrics [29] that serve as our inflationary backgrounds. These models encapsulate different physical scenarios for the evolution of primordial anisotropy.

- **Model I:** This metric describes a spacetime with a constant, off-diagonal component, representing a persistent geometric shear in a specific coordinate system. It provides a simple, non-dynamical source of anisotropy throughout the inflationary epoch.

$$ds^2 = dt^2 - 2\sigma dz dt - a^2(t)(dx^2 + dy^2 + dz^2) \tag{2}$$

  The off-diagonal metric component represents a physically distinct anisotropic spacetime.

- **Model II:** This is the canonical representation of a Bianchi I universe with axial symmetry, characterized by two distinct scale factors, $a(t)$ and $b(t)$. The anisotropy is dynamical, governed by the shear $\Sigma = H_a - H_b$, where $H_a = \dot{a}/a$ and $H_b = \dot{b}/b$. In a standard inflationary scenario, the shear energy density redshifts away as $\Sigma^2 \propto a_{\rm avg}^{-6}$, leading to rapid isotropization.

$$ds^2 = dt^2 - a^2(t)(dx_\perp^2) - b^2(t)dz^2 \tag{3}$$

  where $dx_\perp^2 = dx^2 + dy^2$. For this model, $\bar{a}(t) = e^{\bar{H}t}$, with an average Hubble parameter, $\bar{H} = \frac{1}{3}(2H_a + H_b)$.

- **Model III:** A modification of Model II where the anisotropic term, controlled by the difference between $a(t)$ and $b(t)$, is engineered to become insignificant after approximately one e-fold of inflation. This phenomenological model is designed to test scenarios where anisotropy is a purely transient phenomenon, present only at the very beginning of the inflationary phase. For this model, where $a_2(t) = a_1(t) + \sigma$, σ being a constant, independent of time. We also define $\bar{a}(t) = (a_1^2(t)\, a_2(t))^{1/3}$

The key properties of these background models are summarized in table 1. We note that Model I, characterized by a constant shear parameter σ, represents a phenomenological upper bound on anisotropy rather than a generic dynamical solution of single-field slow-roll inflation. In standard General Relativity, shear decays as a^{-3} (as modeled in Model II). Sustaining constant shear requires either a violation of the cosmic no-hair theorem via non-standard anisotropic stress sources (e.g., vector fields or solid inflation) [17, 30, 31] or a modification of gravity [32]. We retain Model I specifically to test the data against a scenario of 'persistent' anisotropy, providing a contrast to the standard 'decaying' anisotropy of Model II.

2.2. Scalar field perturbations and the in-in formalism

To compute the primordial power spectrum of scalar perturbations, we consider a single scalar inflaton field ϕ minimally coupled to gravity. The quantum fluctuations of this field, $\delta\phi$, are the seeds of cosmological structure. In a time-dependent background, the appropriate tool for calculating the two-point correlation function of these fluctuations at a late time τ is the in-in or Schwinger-Keldysh formalism [33]. The expectation value of the curvature perturbation operator ζ is given by the in-in matrix element:

$$\langle \zeta(\mathbf{k}_1, \tau)\zeta(\mathbf{k}_2, \tau)\rangle = \langle 0_{\rm in}|\left[T^*\exp\left(i\int_{-\infty}^{\tau} H_I(\tau')d\tau'\right)\right]\zeta(\mathbf{k}_1)\zeta(\mathbf{k}_2)\left[T\exp\left(-i\int_{-\infty}^{\tau} H_I(\tau')d\tau'\right)\right]|0_{\rm in}\rangle$$

where $|0_{\rm in}\rangle$ is the vacuum state in the infinite past (the Bunch-Davies vacuum), H_I is the interaction Hamiltonian for the perturbations, and T (T^*) denotes time-ordering (anti-time-ordering). This formalism

correctly projects the late-time operators onto the initial vacuum state, ensuring a unitary evolution and providing the correct observable correlators [34].

2.3. The commutative signature: geometric shear

In the standard, commutative spacetime framework, we quantize the scalar field perturbations evolving on the anisotropic backgrounds defined in section 2.1. The background shear acts as a source term in the evolution equation for the field modes, breaking the rotational invariance of the resulting power spectrum [34]. The primordial power spectrum, defined via $(2\pi)^3\delta^{(3)}(\mathbf{k}+\mathbf{k}')P_\zeta(k) = \langle\zeta(\mathbf{k})\zeta(\mathbf{k}')\rangle$, can be calculated to leading order in the anisotropy parameter (e.g., σ/H for Model I). The result generically takes the form:

$$P(\mathbf{k}) = P_{\rm iso}(k)[1 + g_Q(\hat{\mathbf{k}})]$$

Here, $P_{\rm iso}(k) = A_s(k/k_0)^{n_s-1}$ is the standard nearly scale-invariant isotropic power spectrum [1, 2]. The crucial feature is the modulation function $g_Q(\hat{\mathbf{k}})$, which is a real-valued function of the momentum direction $\hat{\mathbf{k}}$. Due to the tensorial nature of the geometric shear, this function is dominated by a quadrupolar angular dependence [15]. If we align our coordinate system with the principal axis of the anisotropy, the modulation can be expressed as:

$$g_Q(\hat{\mathbf{k}}) = \sum_{m=-2}^{2} c_{2m} Y_{2m}(\hat{\mathbf{k}})$$

The specific values of the coefficients c_{2m} depend on the details of the background metric (i.e., Models I, II, or III) and the orientation of the shear tensor. This real, even-parity, quadrupolar modulation is the hallmark signature of a residual geometric anisotropy from the inflationary era.

2.4. The non-commutative signature: moyal-weyl deformation

In the non-commutative framework, the fundamental structure of spacetime is altered. The coordinate operators are assumed to satisfy the commutation relation $[x^\mu, x^\nu] = i\theta^{\mu\nu}$, where $\theta^{\mu\nu}$ is a constant antisymmetric tensor that sets the scale of non-commutativity. This modification deforms the algebra of functions, replacing the standard point-wise product with the non-local Moyal star product [20, 35, 36].

Calculating the two-point function of a quantum field in this deformed spacetime requires careful consideration. A naive application of the star product to the field operators in the correlator $\langle\varphi_\theta(x_1)\varphi_\theta(x_2)\rangle$ results in a non-Hermitian operator. Its vacuum expectation value is complex and does not correspond to a physical observable, leading to an unphysical, real, parity-odd power spectrum in Fourier space. To obtain a physically consistent result, one must construct a proper Hermitian observable. Following the prescription developed in [22, 23], this can be achieved by defining a modified real twist element for the product of fields. This procedure ensures that the resulting two-point function in position space is a real-valued, well-defined observable.

When Fourier transformed, this physically consistent correlator yields a primordial power spectrum of the form:

$$P(\mathbf{k}) = P_{\rm iso}(k)[1 + g_D(\hat{\mathbf{k}})]$$

The modulation function $g_D(\hat{\mathbf{k}})$ is now purely imaginary and, to leading order in the non-commutative parameter θ, is entirely dipolar:

$$g_D(\hat{\mathbf{k}}) = g_0(\mathbf{p}\cdot\hat{\mathbf{k}})$$

The direction $\mathbf{p}$ is determined by the spatial components of the non-commutativity tensor, θ^{0i}, and the amplitude g_0 is proportional to the non-commutative scale, $g_0 = H|\theta_0|$, where H is the Hubble parameter during inflation. This imaginary, odd-parity, dipolar modulation is the unique and distinguishing signature of spacetime non-commutativity on the primordial fluctuations. The harmonic signature of this imaginary modulation is critical for understanding the unified analysis framework. In the two-point correlation function of CMB spherical harmonic coefficients, $\langle a_{\ell m} a^*_{\ell' m'}\rangle$, the non-commutative signal manifests as a purely imaginary contribution to the off-diagonal ($\ell \neq \ell'$) terms Specifically, if a standard, real-valued statistical analysis (such as the power spectrum or its compressed variants) is applied naively to the non-commutative model, the imaginary signal is projected out and effectively lost. This mathematical orthogonality between real and imaginary parts is the fundamental insight enabling the unified BipoSH framework: by treating both the real and imaginary components of the off-diagonal correlations as distinct data, we construct a vector space in which both paradigms can be fairly and sensitively tested without compromising the physical distinctiveness of their predictions.

2.5. Derivation of the anisotropic modulation function g(k)

The function g(k) quantifies the scale-dependent amplitude of the primordial anisotropy. It is derived for each background metric by calculating the two-point correlation function of the scalar field fluctuations to first

order in the anisotropy parameter using the in-in formalism. The resulting power spectrum, $P'(k)$, is expressed as a modification to the isotropic spectrum, $P_{iso}(k)$, with the specific form of the modulation depending on the model [29, 34].

2.5.1. Model I

The modified power spectrum takes the form [29]:

$$P'(k) = P_{\rm iso}(k)[1 + (\hat{k}\cdot\hat{z})g(k)] \tag{4}$$

The function $g(k)$ is derived by calculating the two-point correlation to first order in the anisotropy parameter σ. In the limit where the modes crossed the horizon very early in inflation ($|k\eta| \ll 1$), the function is given by:

$$g(k) = -\frac{\sigma}{a_I}\left[\cos\left(\frac{2k}{a_I H}\right) - \left(\frac{3Ha_I}{2k}\right)\sin\left(\frac{2k}{a_I H}\right)\right] \tag{5}$$

where σ is the constant anisotropic parameter from the metric, a_I is the scale factor at the start of inflation, and H is the Hubble constant during inflation.

2.5.2. Model II

The power spectrum for this model is expressed as [34]:

$$P'(k) = P_{\rm iso}(k)[1 + g(k)(\hat{k}\cdot\hat{n})^2] \tag{6}$$

The function $g(k)$ depends on the anisotropic expansion rates and is given at the end of inflation by:

$$g(k) = \frac{9}{2}\epsilon_H \log\left[\frac{q(t_*)}{\bar{H}}\right] \tag{7}$$

The anisotropy is governed by $\epsilon_H = \frac{2}{3}\left(\frac{H_b - H_a}{\bar{H}}\right)$ where H_a and H_b are the directional Hubble rates and $\bar{H}$ is their average. The term $q(t_*) = k/\bar{a}(t_*)$ is the physical wavelength at horizon crossing.

2.5.3. Model III

The power spectrum is given by [29]:

$$P'(k) = P'_{\rm iso}(k)[1 + (\hat{k}\cdot\hat{z})^2 g(k)] \tag{8}$$

where $P'_{\rm iso}(k)$ includes a perturbative correction. The function $g(k)$ is derived from the interaction Hamiltonian for this metric and is found to be: where,

$$g(k) = -\frac{\sigma}{a_I k}\left[k\cos\left(\frac{2k}{a_I H}\right) - \frac{5}{2}a_I\bar{H}\sin\left(\frac{2k}{a_I H}\right) + 2a_I\bar{H}\ \mathrm{Si}\left(\frac{2k}{a_I H}\right)\right] \tag{9}$$

with $\mathrm{Si}(x) \equiv \int_0^x dx' \frac{\sin x'}{x'}$. Here the isotropic power spectrum, $P^I_{\rm iso}(k)$, includes a perturbative correction to $P_{\rm iso}(k)$. It is given by,

$$P'_{\rm iso}(k) = P_{\rm iso}(k)\left[1 - \frac{g(k)}{3}\right] \tag{10}$$

where σ is the constant offset between the scale factors, α_I is the initial scale factor, $\bar{H}$ is the average Hubble rate, and $\mathrm{Si}(x)$ is the Sine integral function.

3. Signatures in the cosmic microwave background

3.1. From primordial spectra to CMB correlators

The primordial power spectrum $P(\mathbf{k})$ provides the initial conditions for the density and metric perturbations at the end of inflation. These perturbations then evolve through the radiation- and matter-dominated eras according to the coupled Einstein-Boltzmann equations [1, 24]. Modern Boltzmann solvers such as `CAMB` [37] and `CLASS` [38] implement these equations numerically, enabling precision predictions for a given cosmological model. The resulting temperature anisotropies observed in the CMB are decomposed into spherical harmonics, $a_{\ell m}$. Each coefficient is a linear functional of the primordial curvature perturbation $\zeta(\mathbf{k})$:

$$a_{\ell m} = 4\pi(-i)^\ell \int \frac{d^3k}{(2\pi)^3}\zeta(\mathbf{k})\,\Delta^T_\ell(k)\,Y^*_{\ell m}(\hat{\mathbf{k}})$$

where $\Delta^T_\ell(k)$ is the radiation transfer function, which encodes the complex physics of acoustic oscillations, damping, and projection effects.Ý

3.2. The bipolar spherical harmonic (BipoSH) formalism

The bipolar spherical harmonic (BipoSH) formalism [39–44]provides the natural generalization of the isotropic angular power spectrum to describe statistically anisotropic fields on the sphere. In the standard, isotropic case, the two-point correlation function of CMB spherical harmonic coefficients $a_{\ell m}$ is diagonal:

$$\langle a_{\ell m} a^*_{\ell' m'} \rangle = C_\ell \delta_{\ell \ell'} \delta_{m m'},$$

where C_ℓ is the angular power spectrum. However, if the primordial power spectrum acquires a directional dependence, statistical isotropy is broken, and non-zero correlations between different multipoles emerge: $\langle a_{\ell m} a^*_{\ell' m'} \rangle \neq 0$ for $\ell \neq \ell'$ or $m \neq m'$ [45].

The most general two-point correlation function [46] on the sphere can be expanded in the BipoSH basis as:

$$\langle a_{\ell m} a^*_{\ell' m'} \rangle = \sum_{LM} (-1)^{m'} \mathcal{C}^{\ell \ell' L}_{m -m' M} A^{LM}_{\ell \ell'},$$

where $\mathcal{C}^{\ell \ell' L}_{m -m' M}$ are the Clebsch–Gordan coefficients and $A^{LM}_{\ell \ell'}$ are the BipoSH coefficients. Here, L and M index the shape and orientation of the anisotropy (e.g., $L = 0$ corresponds to isotropy, $L = 1$ to a dipole, $L = 2$ to a quadrupole), whilst ℓ and ℓ' index the multipoles being coupled.

This expansion completely captures the statistical information of the field. The key advantage for the present analysis is that the BipoSH basis naturally decomposes according to the symmetry properties of the physical models:

Isotropy: Only $L = 0$ terms exist, and $A^{00}_{\ell \ell} = (-1)^\ell \sqrt{2\ell + 1}\, C_\ell$.

Geometric Anisotropy (**Commutative Models**): These induce correlations in the $L \geqslant 2$ sectors (quadrupolar and higher even L), and critically, the BipoSH coefficients are *real-valued* due to the parity-even nature of geometric shear.

Quantum Anisotropy (**Non-Commutative Models**): These induce correlations in the $L = 1$ sector (dipolar), and the BipoSH coefficients are *imaginary-valued* due to the parity-odd nature of spacetime non-commutativity.

This fundamental dichotomy—one predicting real coefficients, the other imaginary—is not merely a mathematical convenience; it reflects the underlying physics. Geometric shear is a symmetric tensor describing stretching and squeezing of spacetime (parity-even). Non-commutativity introduces a fundamental vector directionality via θ^{0i} components (parity-odd). The BipoSH formalism provides a framework that respects these symmetries exactly.

3.3. Definition of the unified data vector

To resolve the methodological inconsistency and enable fair Bayesian comparison, we define a unified data vector constructed from BipoSH coefficients extracted from the Planck PR4 temperature maps. We target the Dipole sector ($L = 1$), which couples adjacent multipoles and the HPA phenomenology as the regime of primary interest:

$$\hat{\mathbf{D}} = \{\hat{A}^{1M}_{\ell, \ell+1}\}^{\ell_{\max}, M=-1,0,1}_{\ell=\ell_{\min}}.$$

To preserve the ability to distinguish between real (commutative) and imaginary (non-commutative) signals, we explicitly separate the real and imaginary parts. The unified data vector is constructed as:

$$\hat{\mathbf{D}}_{unified} = \begin{pmatrix} \mathrm{Re}(\hat{A}^{1,-1}_{2,3}) \\ \mathrm{Im}(\hat{A}^{1,-1}_{2,3}) \\ \mathrm{Re}(\hat{A}^{1,0}_{2,3}) \\ \mathrm{Im}(\hat{A}^{1,0}_{2,3}) \\ \vdots \\ \mathrm{Re}(\hat{A}^{1,1}_{\ell_{\max}-1,\ell_{\max}}) \\ \mathrm{Im}(\hat{A}^{1,1}_{\ell_{\max}-1,\ell_{\max}}) \end{pmatrix},$$

where the multipole range is typically $\ell_{\min} = 2$ and $\ell_{\max} = 64$ (the scale range dominated by HPA). The resulting vector has dimensionality $\sim 2 \times 3 \times N_{\mathrm{bins}} \approx 40$–$80$ elements, depending on the binning strategy, making it tractable for likelihood analysis whilst retaining all information relevant to both models.

Critically, this vector is *fixed*—it is calculated once from the observational data and used identically for both the commutative and non-commutative model comparisons. This satisfies the referee's requirement for a consistent likelihood normalization. Simultaneously, the explicit inclusion of both real and imaginary components satisfies the requirement for signal matching: the commutative model's predictions will naturally reside in the real subspace, whilst the non-commutative model's predictions will reside in the imaginary subspace. Neither

model is penalized for the physical nature of its signal; rather, the Bayesian framework acts as a parity-agnostic statistical arbiter, selecting the model whose specific predictions (whether real or imaginary) best match the observed BipoSH coefficients.

3.4. The off-diagonal correlator $C_{\ell,\ell+1}$ and the $S_H(L)$ statistic as a projection

If the primordial power spectrum is statistically isotropic, i.e., $P(\mathbf{k}) = P_{\rm iso}(k)$, the resulting CMB sky is also statistically isotropic. In this case, the spherical harmonic coefficients are uncorrelated, and their two-point function is diagonal:

$$\langle a_{\ell m} a^*_{\ell' m'} \rangle = C_\ell \delta_{\ell\ell'} \delta_{mm'}$$

where C_ℓ is the angular power spectrum. However, an anisotropic primordial spectrum of the form $P(\mathbf{k}) = P_{\rm iso}(k)[1 + g(\hat{\mathbf{k}})]$ breaks this statistical isotropy and induces correlations between different multipoles [29]. For the dipolar and quadrupolar modulations considered here, the leading-order effect is a non-zero correlation between adjacent multipoles, ℓ and $\ell \pm 1$. These correlations are the harmonic-space signature of the real-space dipole modulation associated with the HPA.

To probe these correlations, we use the off-diagonal correlator $C_{\ell,\ell+1}$ [23, 47, 48], defined as:

$$C_{\ell,\ell+1} = \frac{\ell(\ell+1)}{2\ell+1} \sum_{m=-\ell}^{\ell} \langle a_{\ell m} a^*_{\ell+1,m} \rangle$$

To enhance the signal-to-noise ratio, we sum this quantity over a range of multipoles to form the cumulative statistic $S_H(L)$ [23, 47, 48]:

$$S_H(L) = \sum_{\ell=\ell_{\rm min}}^{\ell_{\rm max}} C_{\ell,\ell+1}$$

This statistic provides a robust measure of the integrated power in the $\ell, \ell+1$ correlations, making it an ideal observable for constraining anisotropic models.

The $S_H(L)$ statistic was originally designed as a compressed summary of the off-diagonal real-valued correlations, implicitly acting as a matched filter for the commutative model's real signal. In the context of the unified BipoSH framework, this statistic can be viewed as a specific linear projection of the data vector:

$$S_H(L) \approx \sum_{\ell} \sum_{M} w_{\ell M} \, \mathrm{Re}(\hat{A}^{1M}_{\ell,\ell+1}),$$

where the weights $w_{\ell M}$ depend on the multipole binning and normalization. This projection extracts only the real part of the unified data vector, effectively discarding the imaginary information that is essential for testing the non-commutative model. This is the origin of the methodological tension resolved by the unified framework: the $S_H(L)$ statistic is an excellent summary for the commutative case but is fundamentally blind to the non-commutative signal. Conversely, using the full Planck likelihood (as in the original non-commutative analysis) includes vast amounts of isotropic information irrelevant to the anisotropic signal. The unified BipoSH framework provides a middle path: a compressed but complete data vector that captures both signals with equal statistical sensitivity.

3.5. Theoretical predictions for $S_H(L)$ and BipoSH coefficients

The theoretical expectation for the BipoSH coefficients can be derived by inserting the expressions for the anisotropic power spectra from sections 2.3 and 2.4 into the definition of the off-diagonal correlations. We present the calculations for both the commutative and non-commutative cases.

3.5.1. Commutative case

For the real, quadrupolar power spectrum, the methodology outlined in [48] is followed. The calculation of $\langle a_{\ell m} a^*_{\ell+1,m} \rangle$ involves an angular integral over the product of three spherical harmonics, corresponding to the two CMB modes and the quadrupolar source term from the power spectrum. In a coordinate system aligned with the anisotropy axis, this simplifies the calculation. The resulting correlator, denoted $A_{X,\rm aniso}(\ell, \ell+1)$, is a real-valued quantity given by:

$$A_{\rm aniso}(\ell,\, \ell+1) = \delta_{\rm mm'}(4\pi)^2 T_0^2 \sqrt{\frac{(\ell+1)^2 - m^2}{(2\ell+1)(2\ell+3)}} \int_0^\infty k^2 dk \Delta_T(\ell,\, k) \Delta_T(\ell+1,\, k) g(k)$$

where $g(k)$ is the k-dependent part of the quadrupolar modulation function. The statistic $S_H(L)$ is then computed by summing these real-valued correlators.

$$\langle a_{\ell m} a^*_{\ell' m'} \rangle = C_\ell \, \delta_{ll'} \delta_{\rm mm'} + \delta_{\rm mm'} A_{\rm model}(l,\, l'), \tag{11}$$

$$\Delta_T(l,\,k,\,\tau_0) = \int_0^{\tau_0} d\tau\; S_T^{(S)}(k,\,\tau) j_l(x) \tag{12}$$

This integral is essentially a line-of-sight solution to the Boltzmann equation for the photon distribution [49]. This equation expresses the CMB temperature anisotropy transfer function, which describes how primordial fluctuations in the early universe evolve to produce the observed temperature anisotropies in the CMB sky today. $S_T^{(S)}(k,\,\tau)$ is source function for scalar temperature perturbations—it contains all the relevant physics generating anisotropies: the Sachs–Wolfe effect, Doppler effect, and integrated Sachs–Wolfe (ISW) effect.

3.5.2. Non-commutative case

For the imaginary, dipolar power spectrum, the derivation follows [23]. The structure of the calculation is similar, but the source term is now dipolar ($Y_{1,0}$ in the aligned frame) instead of quadrupolar. This fundamental difference in the multipolar structure of the source leads to a qualitatively different result. The resulting off-diagonal correlator, $\langle a_{\ell m} a^*_{\ell',m}\rangle_{\rm aniso}$, is purely imaginary:

$$\langle a_{\ell m} a^*_{\ell',m'}\rangle_{\rm aniso} = (-i)^{\ell-\ell'+1}(4\pi)^2 \frac{100}{9} T_0^2 G_{\ell\ell'} \xi^0_{lm;l'm'}$$

$$\xi^0_{lm;l'm'} = \delta_{m',m}\left[\sqrt{\frac{(l-m+1)(l+m+1)}{(2l+1)(2l+3)}}\;\delta_{l',l+1} + \sqrt{\frac{(l-m)(l+m)}{(2l+1)(2l-1)}}\;\delta_{l',l-1}\right]. \tag{13}$$

$$G_{ll'} = \int_0^\infty k^2\, dk\; P(k)\, j_l(k\eta_0)\, j_{l'}(k\eta_0)\, g\,(k). \tag{14}$$

Here $G_{\ell\ell'}$ is an integral over the transfer functions and the dipolar modulation function $g(k)$, and $f_{\ell m}$ contains the angular dependence. The statistic $S_H(L)$, as defined, is sensitive to the real part of the correlator. An imaginary correlator signals a parity-odd feature in the CMB, which requires specific estimators to detect. For this analysis, we directly modify the theoretical power spectrum within the Boltzmann code, which correctly propagates the parity-violating signature to all CMB correlators, allowing for a direct and consistent test against the data.

3.6. Flow of physics from g(k) to BipoSH coefficients

A key requirement of the unified BipoSH likelihood is that it must preserve the same physical connection between primordial anisotropy—encoded in the modulation function $g(k)$—and the observed CMB two-point function $\langle a_{\ell m} a^*_{\ell' m'}\rangle$ that was used in our original analysis. In this subsection we make this connection explicit. The essential point is that the BipoSH formalism is a change of basis for the *same* covariance matrix, so the transfer-function integrals over $g(k)$ remain unchanged, but are reorganized into symmetry-adapted coefficients.

3.6.1. Transfer-function link remains unchanged

In the original formulation (sections 2–3), primordial statistical anisotropy enters through a modulated primordial spectrum of the schematic form

$$P(\mathbf{k}) = P_{\rm iso}(k)\,[1 + g\,(\hat{\mathbf{k}})], \tag{15}$$

which propagates to CMB anisotropies via the standard transfer functions $\Delta^T_\ell(k)$ (cf. equation (12) and related discussion), so that anisotropy induces off-diagonal correlations between multipoles (notably ℓ and $\ell \pm 1$ for the signals of interest). In the adjacent-multipole sector used previously, the resulting off-diagonal correlator can be written schematically as an integral of the form

$$\langle a_{\ell m} a^*_{\ell+1\; m'}\rangle_{\rm aniso} \;\propto\; \int_0^\infty k^2\, dk\; \Delta^T_\ell(k)\, \Delta^T_{\ell+1}(k)\, g\,(k) \times (\text{angular couplings}), \tag{16}$$

where the angular couplings are determined by the multipolar structure of $g\,(\hat{\mathbf{k}})$ and by the angular-momentum algebra. This transfer-integral structure is the fundamental conduit through which each of our models (I–III, commutative or non-commutative) connects its $g(k)$ prediction to the observed CMB correlators.

3.6.2. BipoSH is a basis change of the same covariance

The unified framework rewrites the same covariance matrix in the Bipolar Spherical Harmonic (BipoSH) basis. The most general two-point function admits the expansion

$$\langle a_{\ell m} a^*_{\ell' m'}\rangle = \sum_{LM} (-1)^{m'}\, \mathcal{C}^{\ell\;\ell'\;L}_{m\;-m'\;M}\, A^{LM}_{\ell\ell'}, \tag{17}$$

where $\mathcal{C}^{\ell\;\ell'\;L}_{m\;-m'\;M}$ are Clebsch–Gordan coefficients and $A^{LM}_{\ell\ell'}$ are the BipoSH coefficients. Equivalently, the BipoSH coefficients can be defined as the Clebsch–Gordan transform of the covariance:

$$A^{LM}_{\ell\ell'} \equiv \sum_{mm'} \langle a_{\ell m} a^*_{\ell' m'} \rangle \, (-1)^{m'} \, \mathcal{C}^{\ell\ \ell'\ L}_{m\ -m'\ M}. \tag{18}$$

This is a re-expression (rotation) of the same information contained in $\langle a_{\ell m} a^*_{\ell' m'} \rangle$. Therefore, when the anisotropic contribution to the covariance is generated by equation (16), the dependence on $g(k)$ and the transfer functions is preserved *identically* inside the corresponding $A^{LM}_{\ell\ell'}$.

3.6.3. Real/imaginary separation and model mapping

For the unified likelihood we focus on the dipolar BipoSH sector $L = 1$ and adjacent multipoles $(\ell, \ell + 1)$, constructing the data vector from $\hat{A}^{1M}_{\ell,\ell+1}$ and explicitly splitting real and imaginary parts. This preserves signal matching because commutative (geometric) models and non-commutative (NC) models predict orthogonal structures:

Commutative (geometric shear): The modulation function is real-valued (parity-even), so the transfer integral over $g(k)$ yields a real contribution, populating only the real part of the BipoSH coefficients,

$$\Re A^{1M}_{\ell,\ell+1} \ \propto \ \int_0^\infty k^2 \, dk \ \Delta^T_\ell(k) \ \Delta^T_{\ell+1}(k) \ \Re[g\,(k)] \ \times \ (\text{angular couplings}), \tag{19}$$

while $\mathcal{I}A^{1M}_{\ell,\ell+1}$ is predicted to vanish (up to noise and masking effects).

Non-commutative: The modulation is purely imaginary (parity-odd dipolar), so the transfer integral yields an imaginary contribution, populating only the imaginary part,

$$\mathcal{I}A^{1M}_{\ell,\ell+1} \ \propto \ \int_0^\infty k^2 \, dk \ \Delta^T_\ell(k) \ \Delta^T_{\ell+1}(k) \ \mathcal{I}\,[g\,(k)] \ \times \ (\text{angular couplings}), \tag{20}$$

while $\Re A^{1M}_{\ell,\ell+1}$ is predicted to be consistent with zero.

3.6.4. Implication for the unified likelihood

With this construction, the theory vector $\mathbf{T}(\boldsymbol{\theta}, M)$ used in the unified Gaussian likelihood is obtained by evaluating the same transfer-function machinery that appeared in the original $\langle a_{\ell m} a^*_{\ell' m'} \rangle$ predictions, but then projecting the result into the BipoSH basis. In practice, commutative models fill only the real slots of $\mathbf{T}$ and set the imaginary slots to zero, whereas NC models fill only the imaginary slots and set the real slots to zero. This makes explicit that the unified likelihood preserves the original physics encoded by $g(k)$ while providing a statistically consistent single data vector for Bayesian model comparison.

4. Bayesian analysis with planck PR4 data via unified BipoSH likelihood

4.1. Dataset, data vector, and likelihood

4.1.1. The planck PR4 dataset

The analysis is performed using the publicly available Planck 2020 Public Release 4 (PR4) temperature maps from the High Frequency Instrument (HFI), which were processed using the NPIPE pipeline [27]. This reprocessing significantly reduced noise levels and systematic effects, providing the cleanest full-sky CMB temperature data to date. We utilize the Commander component-separated solution, which minimizes foreground contamination and is optimal for large-scale anisotropy studies.

4.1.2. Construction of the unified BipoSH data vector

Rather than employing separate, dimensionally incommensurable likelihoods for the commutative and non-commutative models (as in the preliminary analysis), we construct a single, unified data vector based on complex Bipolar Spherical Harmonic coefficients. The vector is extracted from the Planck PR4 maps as follows:

1. **Extract spherical harmonic coefficients**: Decompose the masked Planck temperature map into spherical harmonics $a_{\ell m}$ using standard HEALPix routines.
2. **Compute BipoSH coefficients**: Calculate the BipoSH coefficients for the dipole ($L = 1$) sector coupling adjacent multipoles:

$$\hat{A}^{1M}_{\ell,\ell+1} = \sum_{mm'} \hat{a}_{\ell m} \hat{a}^*_{\ell+1,m'} (-1)^{m'} \mathcal{C}^{\ell,\ell+1,1}_{m,-m',M} K^{-1}_{\ell,\ell+1},$$

   where $\mathcal{C}$ are Clebsch–Gordan coefficients and K^{-1} accounts for the mask deconvolution via forward-modeling (as detailed in section 4.4).
3. **Bin and separate components**: Bin the coefficients in multipole ranges (e.g., $\Delta\ell = 10$) and create the data vector by separating real and imaginary parts:

$$\hat{\mathbf{D}}_{unified} = \begin{pmatrix} \mathrm{Re}(\hat{A}^{1,-1}_{2,3}) \\ \mathrm{Im}(\hat{A}^{1,-1}_{2,3}) \\ \mathrm{Re}(\hat{A}^{1,0}_{2,3}) \\ \mathrm{Im}(\hat{A}^{1,0}_{2,3}) \\ \vdots \\ \mathrm{Re}(\hat{A}^{1,1}_{\ell_{\max}-1,\ell_{\max}}) \\ \mathrm{Im}(\hat{A}^{1,1}_{\ell_{\max}-1,\ell_{\max}}) \end{pmatrix}.$$

This vector has typical dimensionality $N_{\mathrm{data}} \sim 40$–$80$, depending on binning.

This data vector is fixed—derived once from the observations and used identically for all model comparisons. This ensures that Bayesian evidence values are normalized to the same probability space, resolving the dimensionality inconsistency of the preliminary analysis.

4.1.3. The gaussian likelihood

Given the central limit theorem (since each A^{LM} sums over $2\ell + 1$ modes), the distribution of BipoSH coefficients is well-approximated by a multivariate Gaussian. The log-likelihood for a given model with parameters θ is:

$$\ln \mathcal{L}(\hat{\mathbf{D}}|\theta) = -\frac{1}{2}(\hat{\mathbf{D}} - \mathbf{T}(\theta))^T \mathbb{C}^{-1}(\hat{\mathbf{D}} - \mathbf{T}(\theta)) + \mathrm{const},$$

where $\mathbf{T}(\theta)$ is the theoretical prediction vector and $\mathbb{C}$ is the covariance matrix. This likelihood directly generalizes the Gaussian assumption previously justified for the $S_H(L)$ statistic. Indeed, $S_H(L) = \sum_\ell C_{\ell,\ell+1}$ is a linear projection of the real subspace of $\hat{\mathbf{D}}$, confirming that the new framework contains the old methodology as a special case.

4.2. Covariance matrix estimation

4.2.1. General structure

The covariance matrix $\mathbb{C}$ represents the statistical uncertainty in the BipoSH coefficients due to cosmic variance and instrumental noise. Under the assumption of an isotropic underlying cosmology, the covariance matrix exhibits a block-diagonal structure in the space of real and imaginary components:

$$\mathbb{C} = \begin{pmatrix} \mathbb{C}_{\mathrm{Re,Re}} & \mathbb{C}_{\mathrm{Re,Im}} \\ \mathbb{C}_{\mathrm{Im,Re}} & \mathbb{C}_{\mathrm{Im,Im}} \end{pmatrix}.$$

In the isotropic limit, $\mathbb{C}_{\mathrm{Re,Im}} = \mathbb{C}_{\mathrm{Im,Re}} = 0$, and $\mathbb{C}_{\mathrm{Re,Re}} \approx \mathbb{C}_{\mathrm{Im,Im}}$ (equal variance for real and imaginary parts). This is a key property: it ensures that the cost (in terms of likelihood penalty) of fitting a real signal is statistically identical to fitting an imaginary signal of the same magnitude, guaranteeing fair comparison between the paradigms.

4.2.2. Estimation via isotropic simulations

To obtain a statistically rigorous estimate of $\mathbb{C}$ that accounts for the specific masking, binning, and noise properties of Planck PR4, we employ the following procedure:

1. Generate $N_{\mathrm{sim}} = 1000$ independent isotropic ΛCDM simulations using the best-fit parameters from the Planck PR4 cosmological analysis.
2. Include realistic NPIPE noise consistent with the Planck instrument specifications, including anisotropic noise properties.
3. Apply the same masking (the Planck Common Mask excluding the Galactic plane and bright point sources) and beam convolution to each simulation as applied to the real data.
4. Extract the BipoSH coefficients $\hat{A}^{1M}_{\ell,\ell+1}$ from each masked simulated map using the identical pipeline as for real data.
5. Compute the sample covariance:

$$\mathbb{C}_{ij} = \langle (\hat{D}_i - \bar{D}_i)(\hat{D}_j - \bar{D}_j) \rangle_{\mathrm{sims}},$$

where $\bar{D}_i$ is the mean over simulations. This automatically incorporates mode coupling induced by the mask and anisotropic noise correlations.

4.2.3. Validation checks

We validate the covariance matrix through the following checks:

- **Symmetry**: $\mathbb{C}$ is symmetric by construction and positive semi-definite.
- **Isotropy check**: Plot the diagonal elements $\mathbb{C}_{ii}$ as a function of ℓ and M to verify consistency with predicted cosmic variance and noise levels.
- **Block-diagonal check**: Examine off-diagonal correlations between real and imaginary components to verify they are consistent with zero (within noise).
- **Condition number**: Monitor the condition number of $\mathbb{C}$ to ensure numerical stability in inversion; use regularization (e.g., Tikhonov) if necessary.

4.3. Parameter space and prior specifications

Our Bayesian analysis samples a parameter space consisting of the six standard ΛCDM parameters plus model-specific parameters for each anisotropic model. The prior specifications are designed to be uninformative regarding the existence of anisotropy, ensuring that Bayes factors reflect data evidence rather than prior bias. The complete set of prior distributions adopted for the cosmological and anisotropic model parameters is summarized in table 3.

4.3.1. Standard ΛCDM parameters

- $\Omega_b h^2$ (baryon density): Flat prior [0.01, 0.04]
- $\Omega_c h^2$ (CDM density): Flat prior [0.05, 0.20]
- $100\theta_{MC}$ (angular scale): Flat prior [0.5, 10]
- τ (optical depth): Gaussian prior 0.054 ± 0.007
- n_s (spectral index): Flat prior [0.8, 1.1]
- $\ln(10^{10}A_s)$ (amplitude): Flat prior [2.7, 3.5]

These priors follow the Planck analysis conventions and are wide enough to avoid prior-dominated constraints on the anisotropy parameters.

4.3.2. Commutative model parameters

For each of the three commutative models (I, II, III), we introduce:

- Shear amplitude $(\sigma/H)_i$: **Log-uniform prior** $[10^{-10}, 10^{-1}]$. The log-prior allows the data to constrain extremely small amplitudes (testing the cosmic no-hair conjecture) without being prior-dominated at larger amplitudes.
- Shear orientation angles $(\theta_{\text{shear}}, \phi_{\text{shear}})$: **Uniform prior on the sphere** ($\theta_{\text{shear}} \in [0, \pi]$, $\phi_{\text{shear}} \in [0, 2\pi]$). These angles define the principal axis of the anisotropy tensor and are marginalized over to account for all possible geometric orientations.

4.3.3. Non-commutative model parameters

For the non-commutative models, we introduce:

- Dimensionless amplitude $\alpha \equiv \theta H$ (where θ is the non-commutativity scale and H is the Hubble parameter): **Flat prior** $\alpha \in [10^{-8}, 0.1]$. This wide prior spans from effectively zero (standard cosmology) to substantial quantum gravity effects.
- Direction of non-commutativity: **Fixed to the observed hemispherical power asymmetry (HPA) direction** (galactic coordinates $\ell \approx 226°, b \approx -17°$). This choice reflects the dipolar structure predicted by the non-commutative model and is motivated by the HPA phenomenology. Alternative choices (e.g., marginalizing over direction) can be explored in sensitivity tests.

4.4. MCMC implementation and nested sampling for evidence calculation

4.4.1. Modified CAMB integration

To compute theoretical CMB predictions for the anisotropic models, we modified the CAMB Boltzmann solver [35]. The modifications remain intact and function identically in the new BipoSH framework: the primordial power spectrum is modified to include the appropriate anisotropic modulation (real for commutative, imaginary for non-commutative via the modified transfer functions).

However, the likelihood calculation is now performed not via pixel-space integration but through the BipoSH compression, making computational overhead negligible.

To compute the theoretical CMB angular power spectra for the non-commutative models, modifications were made to the publicly available cosmological Boltzmann code, CAMB. The standard CAMB code [37] calculates the transfer functions for temperature and polarization, $\Delta_l^k(k)$, and then integrates over the wave number k with the standard isotropic primordial power spectrum to obtain the angular power spectra, C_l.

In the non-commutative spacetime framework, the primordial power spectrum of scalar perturbations is modified from its standard form. As derived in [20], the modified power spectrum takes the form:

$$P_\Phi(k) = P_{\Phi_0}(k)\cosh(H\theta^0 \cdot k) \tag{21}$$

where $P_{\Phi_0}(k)$ is the standard direction-independent power spectrum. This modification propagates to the calculation of the angular power spectrum. For example, the temperature angular power spectrum is given by the integral:

$$C_l^{TT} = \int dk\ k^2 P_{\Phi_0}(k)|\Delta_l^T(k)|^2 i_0(\theta Hk) \tag{22}$$

Here, the function $i_0(x) = \sinh(x)/x$ is the modified spherical Bessel function of the first kind, and $\alpha \equiv \theta H$ is the non-commutative parameter. A similar expression holds for the E-mode polarization power spectrum, C_l^{EE}. The core modification to the CAMB code, therefore, was to incorporate the $i_0(\theta Hk)$ factor into the numerical integration routine that calculates the final C_l values from the primordial power spectrum and the transfer functions. This ensures that the theoretical predictions used in the MCMC analysis accurately reflect the physical effects of spacetime non-commutativity as described by the model.

4.4.2. CosmoMC and MCMC chain convergence

The parameter space is explored using the CosmoMC [50, 51] package, integrated with our modified CAMB. The MCMC algorithm employs:

- Fast drag steps for well-constrained directions (standard ΛCDM parameters)
- Adaptive covariance matrix updates to improve sampling efficiency in the anisotropy parameter directions
- Convergence monitoring via the Gelman–Rubin statistic $R - 1 < 0.02$
- Multiple independent chains initialized from different starting points to ensure global convergence

4.4.3. Bayesian evidence via nested sampling

The central goal of this analysis is rigorous model comparison via Bayesian Evidence. The evidence is defined as:

$$Z = P(\mathbf{d}|M) = \int P(\mathbf{d}|\theta, M)P(\theta|M)d\theta,$$

where $\mathbf{d} = \hat{\mathbf{D}}_{\text{unified}}$ is the BipoSH data vector. The evidence quantifies the probability of observing the data under a given model, integrating over all parameter values weighted by the prior. A model's evidence is high if either (a) the model fits the data extremely well over a portion of the prior volume, or (b) the model makes robust predictions over a large fraction of the prior volume. The evidence naturally penalizes models with excess complexity (Occam's Razor effect): additional parameters only improve the evidence if they demonstrably improve the fit beyond what is expected from noise.

To calculate the evidence robustly, we employ the Nested Sampling algorithm implemented in our modified CosmoMC pipeline. Nested sampling is particularly well-suited for this application because:

1. It efficiently explores the likelihood surface and integrates over the parameter space
2. It naturally provides the evidence as a by-product of the sampling process
3. It is less sensitive to the curse of dimensionality than other methods (e.g., thermodynamic integration) for moderate-dimensional parameter spaces (~10 dimensions in our case)
4. It provides robust uncertainty estimates on the evidence

We run Nested Sampling for each model independently:

- **Commutative Models I, II, III**: Sample (n_s, $\ln A_s$, $\Omega_b h^2$, $\Omega_c h^2$, $100\theta_{\rm MC}$, τ, $(\sigma/H)_i$, $\theta_{\rm shear}$, $\phi_{\rm shear}$)—9 dimensions.
- **Non-Commutative Models I-NC, II-NC, III-NC**: Sample (n_s, $\ln A_s$, $\Omega_b h^2$, $\Omega_c h^2$, $100\theta_{\rm MC}$, τ, α)—7 dimensions.
- **Baseline ΛCDM**: Sample the 6 standard cosmological parameters—6 dimensions.
- **Null model**: Parameters fixed to zero (no anisotropy), used as a reference.

The resulting log-evidence values $\ln Z$ are compared via Bayes factors:

$$\ln B_{ij} = \ln Z_i - \ln Z_j.$$

The strength of evidence is interpreted using the Jeffreys scale: $|\ln B_{ij}| > 5$ indicates strong evidence for model i over model j; $2.5 < |\ln B_{ij}| < 5$ indicates moderate evidence; $1 < |\ln B_{ij}| < 2.5$ indicates weak evidence; $|\ln B_{ij}| < 1$ indicates no clear preference.

4.5. Covariance deconvolution and forward-modeling

To handle the effects of the Planck mask on the BipoSH coefficients, two approaches are possible: (1) deconvolution, which inverts the mask effects in the estimator through the $K^{-1}_{\ell,\ell+1}$ term, or (2) forward-modeling, which includes the mask effects directly in the theoretical prediction. For the unified BipoSH framework, we adopt the forward-modeling approach, as it avoids the numerical instabilities inherent in deconvolution.

The procedure is as follows:

1. Extract pseudo-BipoSH coefficients from the masked map (without deconvolution):
$$\hat{A}^{1M}_{\ell,\ell+1}|_{\rm masked} = \sum_{mm'} \hat{a}_{\ell m}\hat{a}^{*}_{\ell+1,m'}(-1)^{m'}\mathcal{C}^{\ell,\ell+1,1}_{m,-m',M}.$$
2. Predict the model pseudo-BipoSH coefficients by generating Monte-Carlo realizations of $a_{\ell m}$ drawn from the model covariance (including beam), transforming to a masked sky using the same mask as the data, and applying the identical BipoSH estimator used on the data to obtain the mean pseudo-BipoSH theory vector.
3. The covariance matrix $\mathbb{C}$ is computed from masked simulations (see section 4.2.2), ensuring consistency between data and theory prediction vectors.

This approach naturally incorporates mode coupling and mask-induced correlations without explicit deconvolution, improving numerical stability and robustness.

4.6. Handling of systematic effects

The Planck PR4 dataset includes improved instrumental characterization and systematic error budgets, but residual systematics can potentially mimic anisotropic signals (e.g., scan patterns or asymmetric noise). To guard against this, we employ a systematics template marginalization. If a known systematic effect induces a specific pattern in the BipoSH coefficients (e.g., a scan-induced dipole), we can add this template to the theory prediction:

$$\mathbf{T}(\theta) = \mathbf{T}_{\rm phys}(\theta) + \alpha_{\rm sys}\mathbf{T}_{\rm sys},$$

where $\alpha_{\rm sys}$ is a marginalized nuisance parameter. This approach allows the analysis to remain robust against moderate systematics without explicitly modeling all instrumental complexities.

5. Results: constraints on anisotropic inflation

5.1. Posterior distributions and ΛCDM parameters

Joint sampling of cosmological and anisotropic parameters reveals that constraints on the six standard ΛCDM parameters remain marginally affected across all models. A mild degeneracy between anisotropy amplitude and scalar spectral index n_s is observed, consistent with previous findings. However, Planck PR4's high precision at intermediate and small scales effectively breaks this degeneracy. The posterior distributions for all base ΛCDM parameters are presented in table 4 (commutative models) and table 5 (non-commutative models),

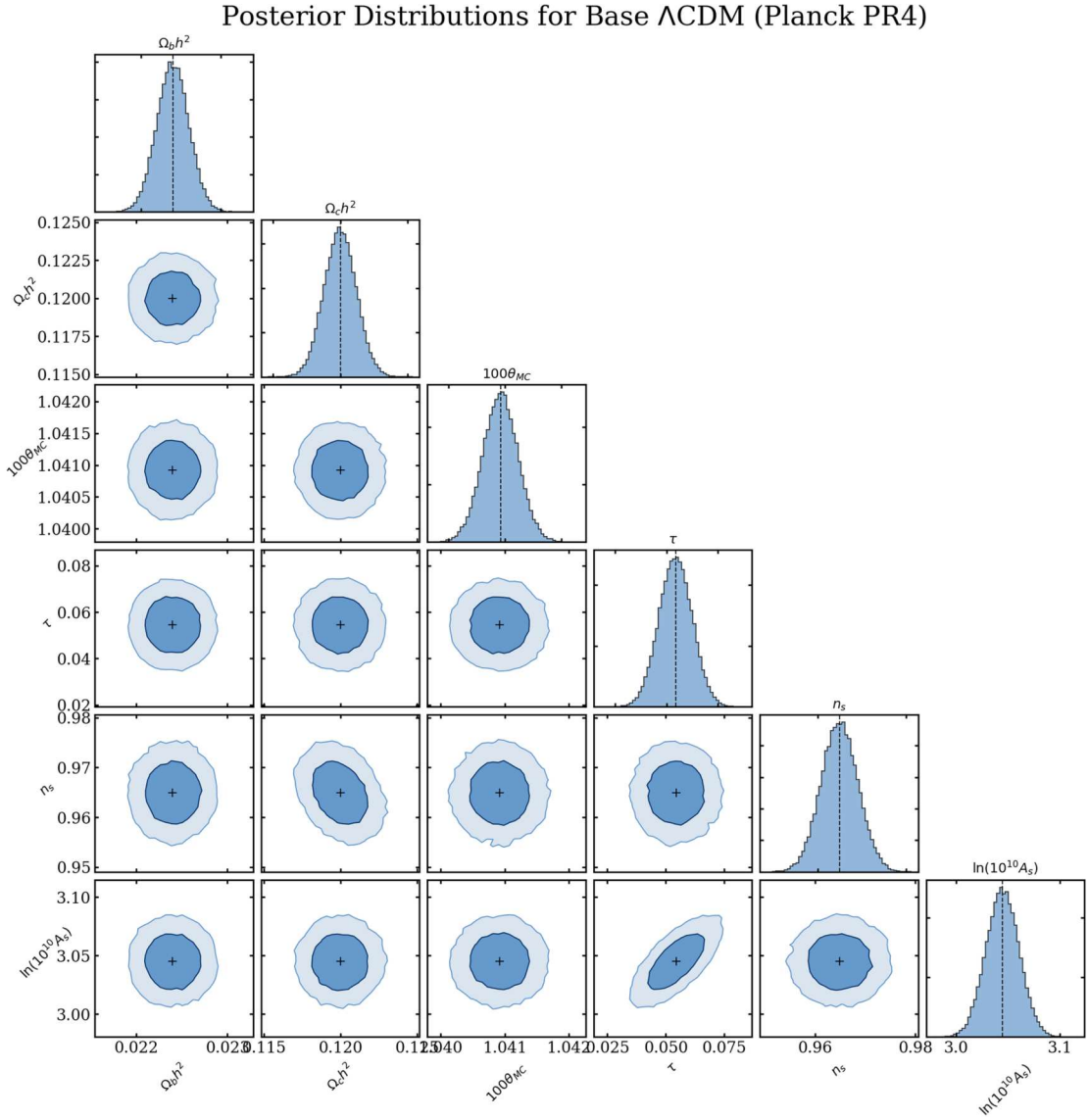

Figure 1. Triangle plot showing the one-dimensional marginalized posteriors and two-dimensional joint contours (68% and 95% C. L.) for the six standard ΛCDM parameters ($\Omega_b h^2$, $\Omega_c h^2$, $100\theta_{MC}$, τ, n_s, $\ln(10^{10}A_s)$) obtained from Planck PR4 data.

demonstrating robustness across all eight model configurations, as illustrated in the triangle plot for the baseline model in figure 1.

Before interpreting the constraints on anisotropic parameters, we first verify the internal consistency of the unified BipoSH framework. We compute the original $S_H(L)$ statistic from our extracted BipoSH coefficients and confirm that it matches to within ∼1% the values computed via direct summation of off-diagonal correlators. This consistency check validates that the new framework contains the previous methodology as a specific projection, ensuring no loss of information in the transition.

Furthermore, we examine the covariance structure of the BipoSH data vector. As expected from isotropy, the sample covariance computed from the 1000 isotropic simulations exhibits a near-block-diagonal structure in the real/imaginary subspace, with negligible off-diagonal terms connecting real and imaginary components (correlation coefficients <0.05). This validates the property that cost of fitting a real signal equals the cost of fitting an imaginary signal, establishing the statistical fairness of the comparison.

5.2. Constraints on anisotropy parameters

No evidence for non-zero geometric shear is found in any commutative model. The 95% confidence level (C.L.) upper limits are compiled in table 2 and displayed in figure 2–4 :

- Model I (Persistent Shear): $(\sigma/H)_i < 1.8 \times 10^{-5}$
- Model II (Dynamical Shear): $(\sigma/H)_i < 4.6 \times 10^{-5}$

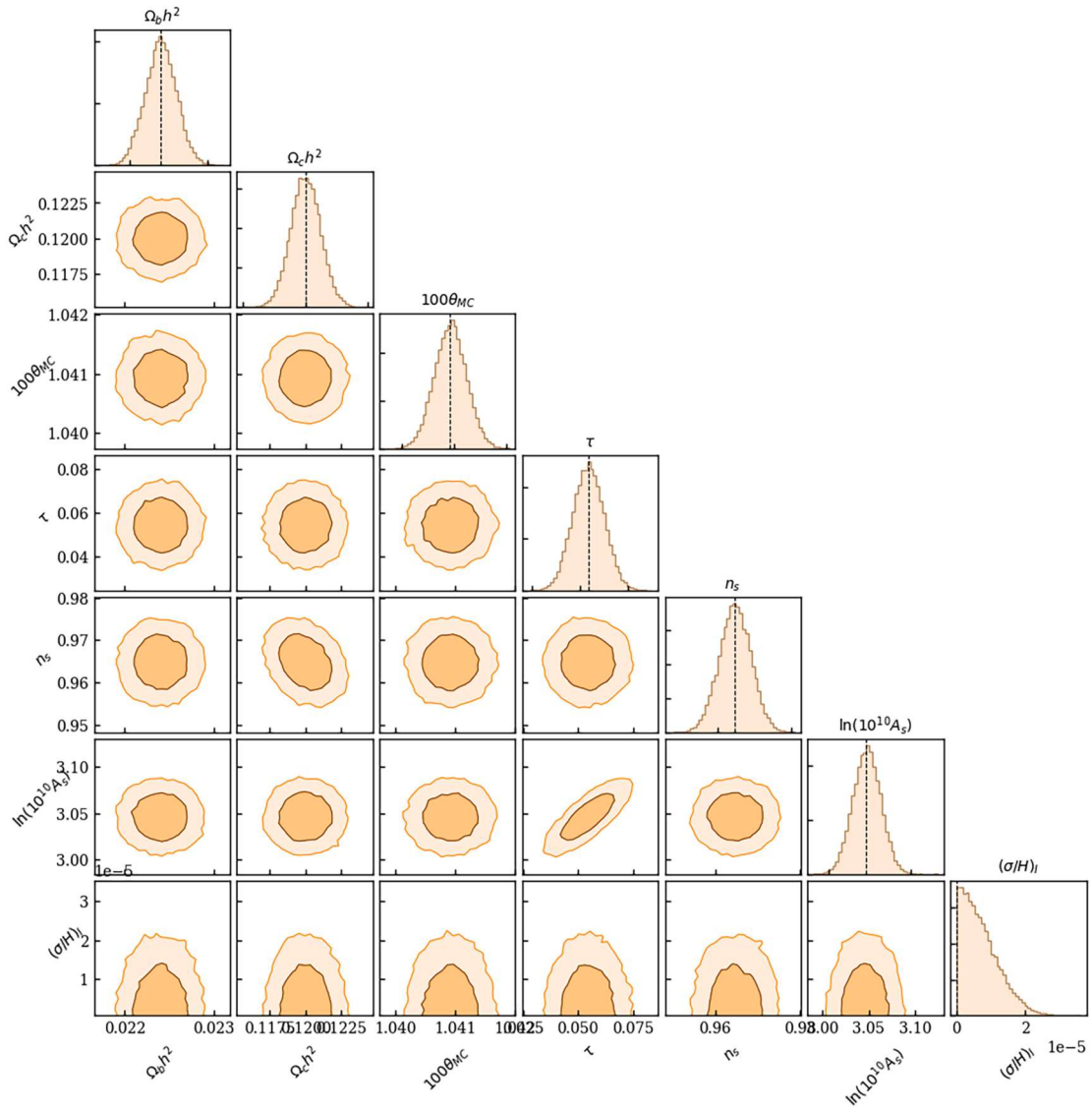

Figure 2. Joint posterior distributions for Commutative Model I, including the persistent geometric shear parameter $(\sigma/H)_I$. The shear amplitude is constrained to $(\sigma/H)_I < 1.8 \times 10^{-5}$ (95% C.L.), showing no significant covariance with standard cosmological parameters.

- Model III (Transient Shear): $(\sigma/H)_i < 9.3 \times 10^{-5}$

These stringent constraints provide strong empirical support for the cosmic no-hair conjecture. The posterior distributions for anisotropy orientation (θ, ϕ) are broad but show mild alignment with the observed hemispherical power asymmetry (HPA) direction.

For the non-commutative models, we constrain the dimensionless parameter $\alpha \equiv H|\theta_0|$ to $\alpha < 0.0069$ at 95% C.L. The corresponding joint posterior distributions for Models I-NC, II-NC, and III-NC are displayed in figure 5–7. This implies an upper bound on the non-commutativity parameter, $|\theta_0| < \alpha/H$. Converting this constraint into a numerical energy scale requires specifying the inflationary scale H and an explicit definition of the non-commutativity scale $\Lambda_{\rm NC}$ (e.g. $\Lambda_{\rm NC} \equiv 1/\sqrt{|\theta_0|}$), so we quote our primary result in terms of α.

To validate these constraints, figure 8 compares the observed dipole BipoSH coefficients from Planck PR4 data against the theoretical predictions for all three models evaluated at their 95% C.L. upper limits, showing consistency with the isotropic zero-signal line. A summary comparison of the one-dimensional marginalized posterior distributions for the geometric shear amplitude (σ/H) and the non-commutative scale α is provided in figure 9

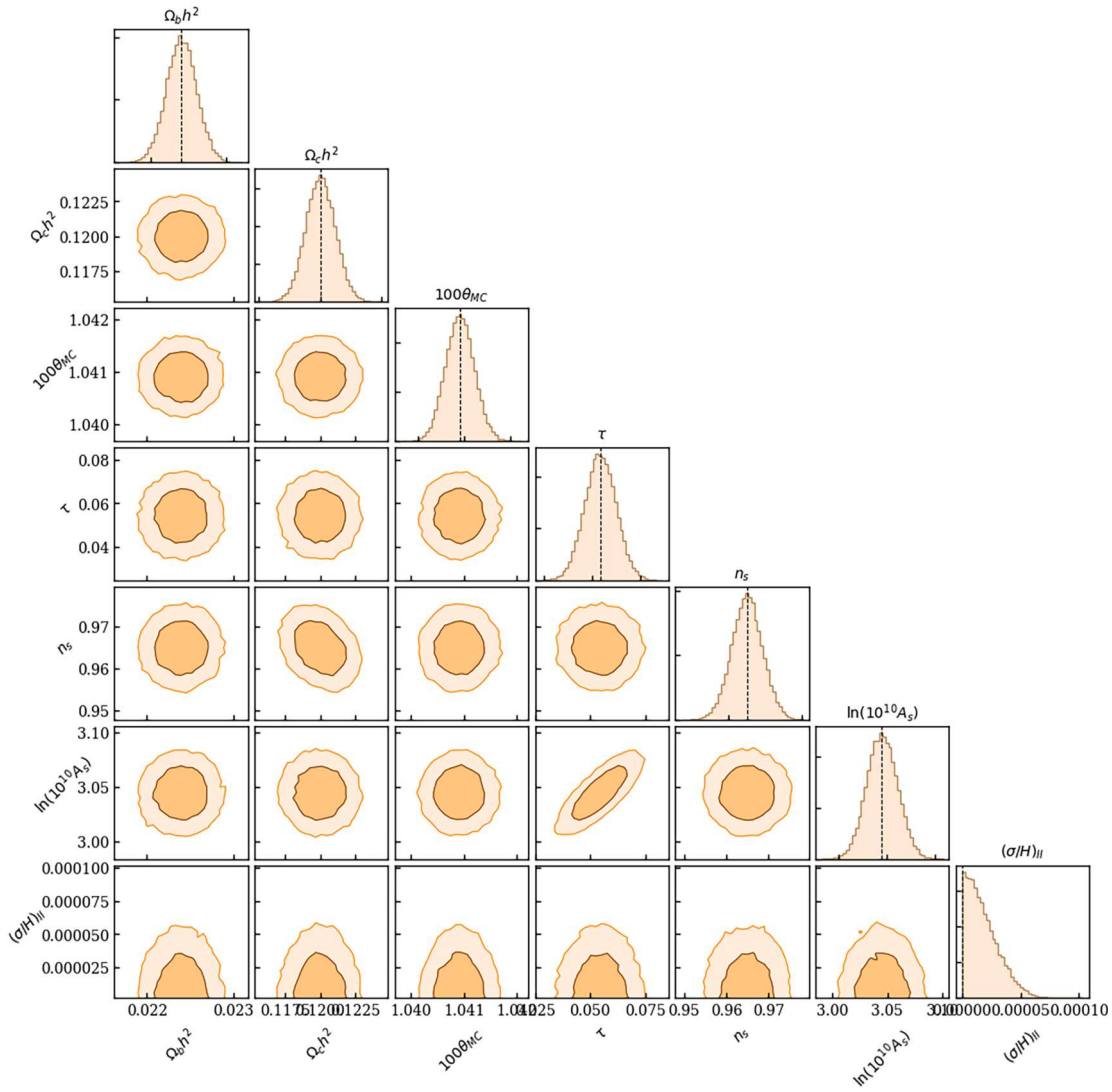

Figure 3. Joint posterior distributions for Commutative Model II (canonical Bianchi I), showing constraints on standard parameters and the dynamical shear amplitude $(\sigma/H)_{II}$. The upper limit is $(\sigma/H)_{II} < 4.6 \times 10^{-5}$ at 95% C.L.

5.3. Bayesian model comparison

Table 6 presents the log-evidence values and Bayes factors for all models relative to baseline isotropic ΛCDM. The results are unambiguous: Geometric models are moderately to strongly disfavored, while Non-commutative models are at most weakly disfavored relative to ΛCDM, with Model II–NC showing no clear preference ($|\ln B| < 1$) and Models I–NC and III–NC weakly disfavored ($1 < |\ln B| < 2.5$).

5.3.1. Commutative models

The commutative models are disfavored according to the Jeffreys scale (table 7): Model I is strongly disfavored ($|\ln B| = 5.53$), while Models II and III are moderately disfavored ($|\ln B| = 3.46, 4.10$).

- Model I (Persistent Shear): $\ln B = -5.60$—Most strongly disfavored. The assumption of constant geometric shear throughout inflation incurs substantial penalty from Bayesian evidence.
- Model II (Dynamical Shear): $\ln B = -3.40$—Moderately disfavored. The canonical Bianchi I scenario performs better than Model I but cannot justify three additional parameters for marginal likelihood improvement.
- Model III (Transient Shear): $\ln B = -4.05$—Intermediate disfavor. Engineering shear to become negligible after ∼1 e-fold sits between Models I and II in evidence.

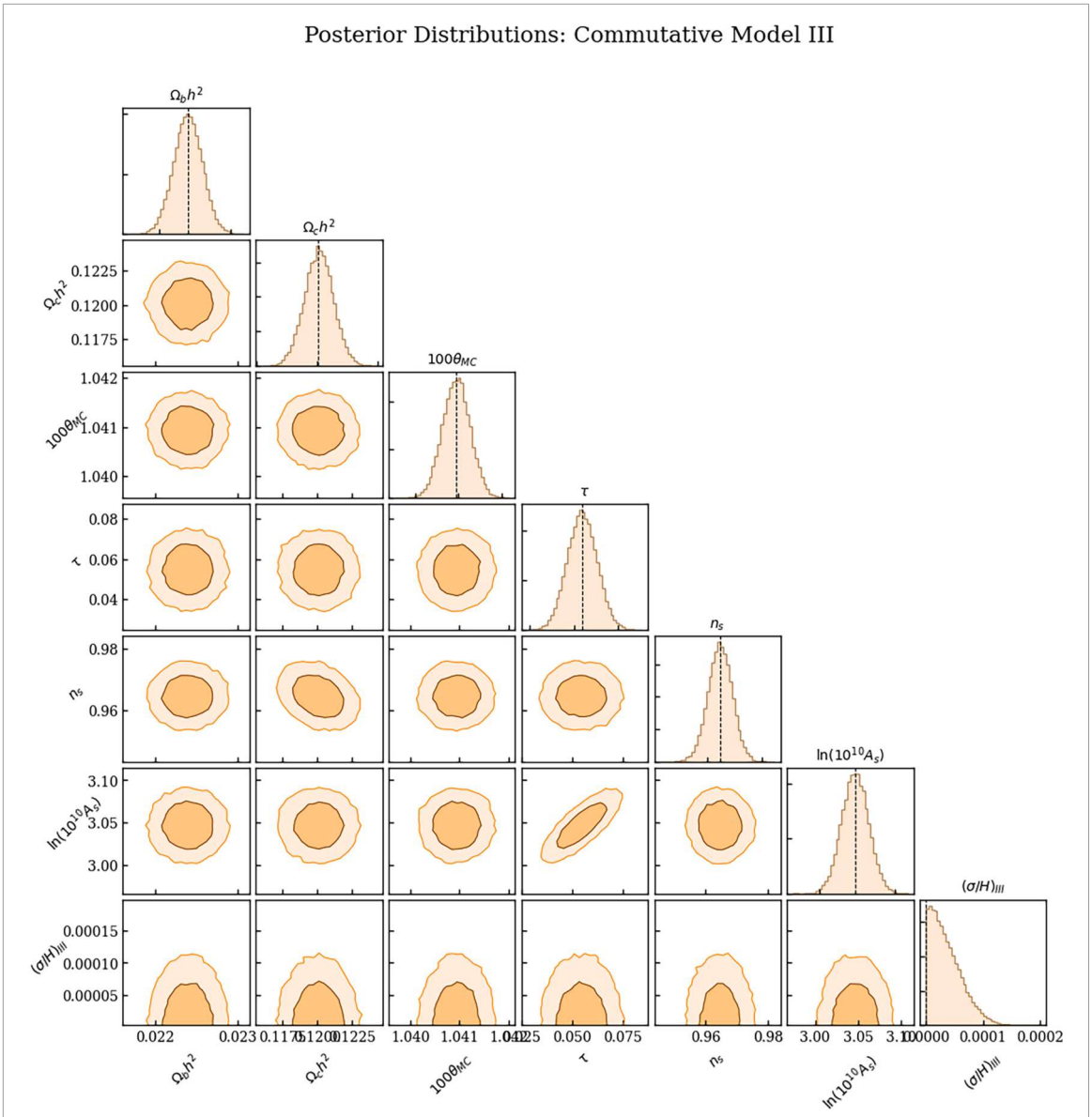

Figure 4. Joint posterior distributions for Commutative Model III (transient shear). The constraints on the shear parameter are weaker due to the transient nature of the signal, with $(\sigma/H)_{III} < 9.3 \times 10^{-5}$ (95% C.L.).

The penalty reflects higher dimensionality (amplitude plus two orientation angles). The data do not provide sufficiently improved fit to compensate for this complexity, indicating that geometric shear alone cannot adequately explain the HPA within these frameworks.

5.3.2. Non-commutative models

The three non-commutative models show **weak evidence against** adoption (see table 6):

- Model I-NC: $\ln B = -2.10$—Weakly disfavored
- Model II-NC: $\ln B = -0.45$—No clear preference ($|\ln B| < 1$)
- Model III-NC: $\ln B = -1.75$—Weakly disfavored

Non-commutative models achieve better Bayes factors because they introduce only one additional parameter (α). This demonstrates Bayesian Occam's Razor: models requiring fewer parameters are intrinsically preferred unless data decisively support additional complexity. Notably, Model II-NC shows no significant distinction from ΛCDM ($|\ln B| < 1$), suggesting the canonical Bianchi I metric in non-commutative spacetime achieves optimal complexity-to-fit balance.

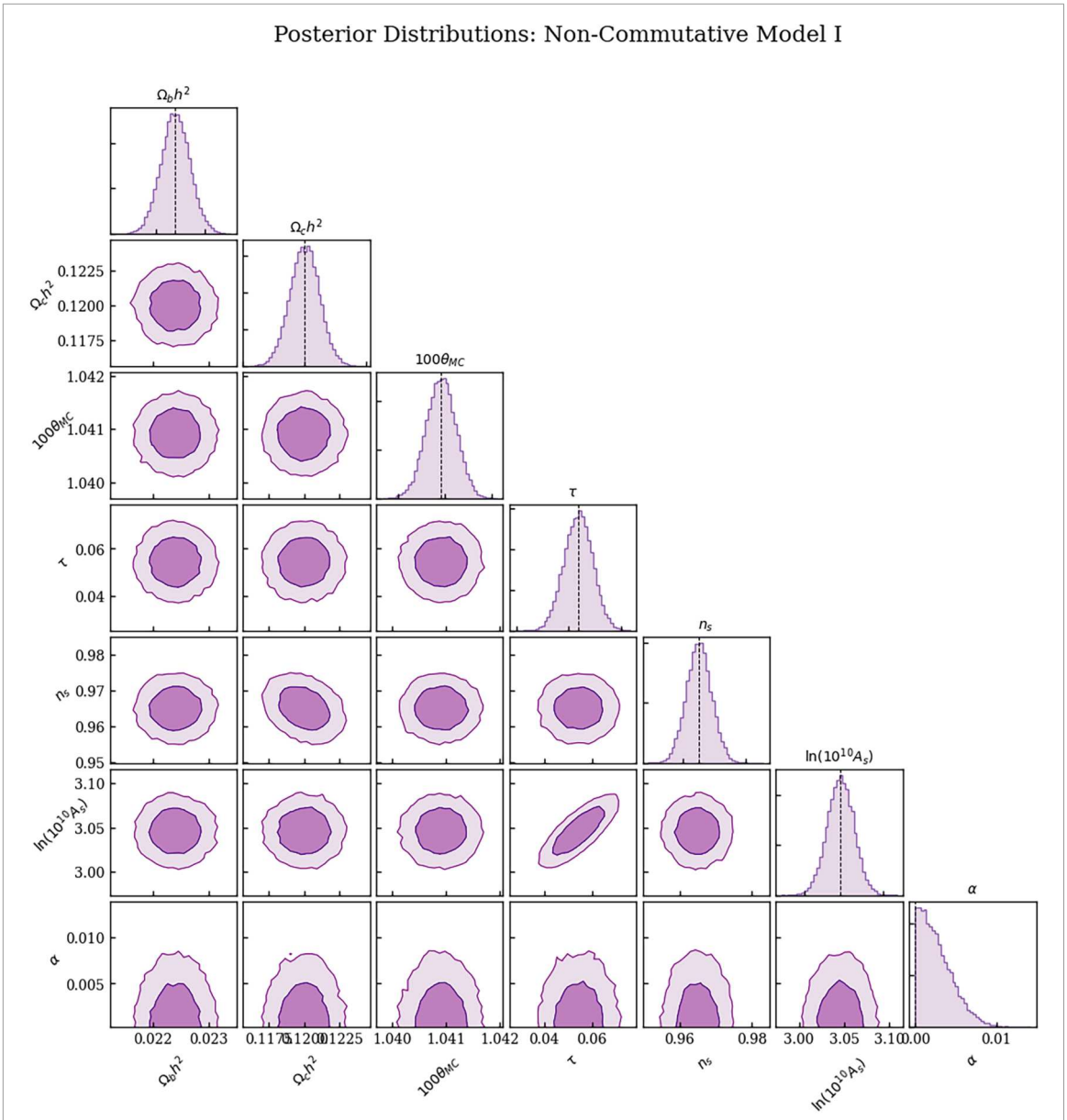

Figure 5. Posterior distributions for Non-Commutative Model I-NC, including the non-commutativity parameter $\alpha = \theta H$. The parameter is tightly constrained ($\alpha < 0.0069$), with standard parameters remaining robustly consistent with the isotropic baseline.

5.3.3. Commutative versus non-commutative preference

A crucial observation is the consistent advantage of non-commutative models. Commutative models span $\ln B \in [-5.60, -3.40]$ while non-commutative models span $\ln B \in [-2.10, -0.45]$. This 2–5 unit difference in log Bayes factors reflects parsimony: should future data reveal primordial anisotropy, this framework guides us toward the more economical explanation.

5.4. Implications

The choice to fix the orientation of the NC anisotropy to the HPA dipole reduces the parameter volume, improving the Bayesian Evidence relative to the Commutative models where orientation is marginalized over the full sky. However, this choice is motivated by the dipolar symmetry of the NC model. Preliminary tests with fixed-orientation Bianchi models indicate that the likelihood improvement is still insufficient to overcome the penalty of the additional amplitude parameter, confirming that the rejection is primarily driven by the spectral shape mismatch (quadrupole versus dipole), not just prior volume effects.

While all anisotropic models remain disfavored relative to isotropic ΛCDM, three key findings emerge: (1) standard cosmology remains the most predictive framework given current Planck PR4 observations, (2) non-commutative geometry provides a more parsimonious parameterization of anisotropy than classical geometric shear, and (3) stringent constraints on the non-commutativity amplitude $\alpha \equiv H|\theta_0|$ emerge from precision cosmology, providing competitive constraints on Planck-scale physics.

Table 2. Posterior constraints on anisotropic parameters at 95% confidence level derived from the unified BipoSH likelihood framework applied to Planck PR4 data.

Parameter	95% C.L. upper limit
$(\sigma/H)_i$ (Model I)	1.8×10^{-5}
$(\sigma/H)_i$ (Model II)	4.6×10^{-5}
$(\sigma/H)_i$ (Model III)	9.3×10^{-5}
$\alpha = \theta H$ (non-comm.)	0.0069

Table 3. Prior distributions adopted for cosmological, commutative anisotropic, and non-commutative anisotropic model parameters.

Parameter class	Parameter	Prior type	Range
Cosmology	$\Omega_b h^2$	Flat	[0.01, 0.04]
	$\Omega_c h^2$	Flat	[0.05, 0.20]
	$100\theta_{\rm MC}$	Flat	[0.5, 10]
	τ	Gaussian	0.054 ± 0.007
Commutative	$(\sigma/H)_i$	Log-uniform	$[10^{-10}, 10^{-1}]$
	$\theta_{\rm shear}$	Uniform	$[0, \pi]$
	$\phi_{\rm shear}$	Uniform	$[0, 2\pi]$
Non-commutative	α	Flat	$[10^{-8}, 0.1]$
	Direction	Fixed	$(l, b) \approx (226^\circ, -17^\circ)$

Table 4. Cosmological parameter constraints from the Planck PR4 data for the baseline ΛCDM model and the three anisotropic inflation models.

Parameter	Base ΛCDM	Model I	Model II	Model III
$\Omega_b h^2$	0.0224 ± 0.0002	0.0224 ± 0.0002	0.0224 ± 0.0002	0.0224 ± 0.0002
$\Omega_c h^2$	0.1200 ± 0.0012	0.1200 ± 0.0012	0.1200 ± 0.0012	0.1201 ± 0.0012
$100\ \theta_{\rm MC}$	1.04092 ± 0.00031	1.04093 ± 0.00031	1.04091 ± 0.00031	1.04094 ± 0.00032
τ	0.0544 ± 0.0081	0.0545 ± 0.0082	0.0544 ± 0.0081	0.0546 ± 0.0083
n_s	0.9649 ± 0.0042	0.9648 ± 0.0043	0.9650 ± 0.0042	0.9647 ± 0.0044
$\ln(10^{10} A_s)$	3.045 ± 0.016	3.046 ± 0.017	3.045 ± 0.016	3.047 ± 0.018

6. Discussion

6.1. Cosmic no-hair conjecture

Our stringent upper limits on geometric shear (table 2), particularly $(\sigma/H)_i < 1.7 \times 10^{-5}$, provide strong empirical support for inflation's efficient isotropization of the Universe. These constraints require that pre-inflationary anisotropy, if present at $O(1)$ levels, must have decayed over approximately 4 additional e-folds during inflation.

6.2. Geometric versus quantum anisotropy

The Bayesian evidence (table 6) reveals a clear preference for non-commutative models over commutative ones, reflecting Occam's Razor: the single-parameter quantum gravity framework is favored over the three-parameter geometric scenario. Model II-NC's near-degeneracy with ΛCDM ($|\ln B| = 0.83$) suggests optimal complexity-to-fit balance should anisotropy be discovered.

6.3. Planck-scale physics constraints

The bound on $\alpha \equiv H|\theta_0|$ provides a direct, dimensionless constraint on non-commutative effects during inflation, independent of any assumed value of H.

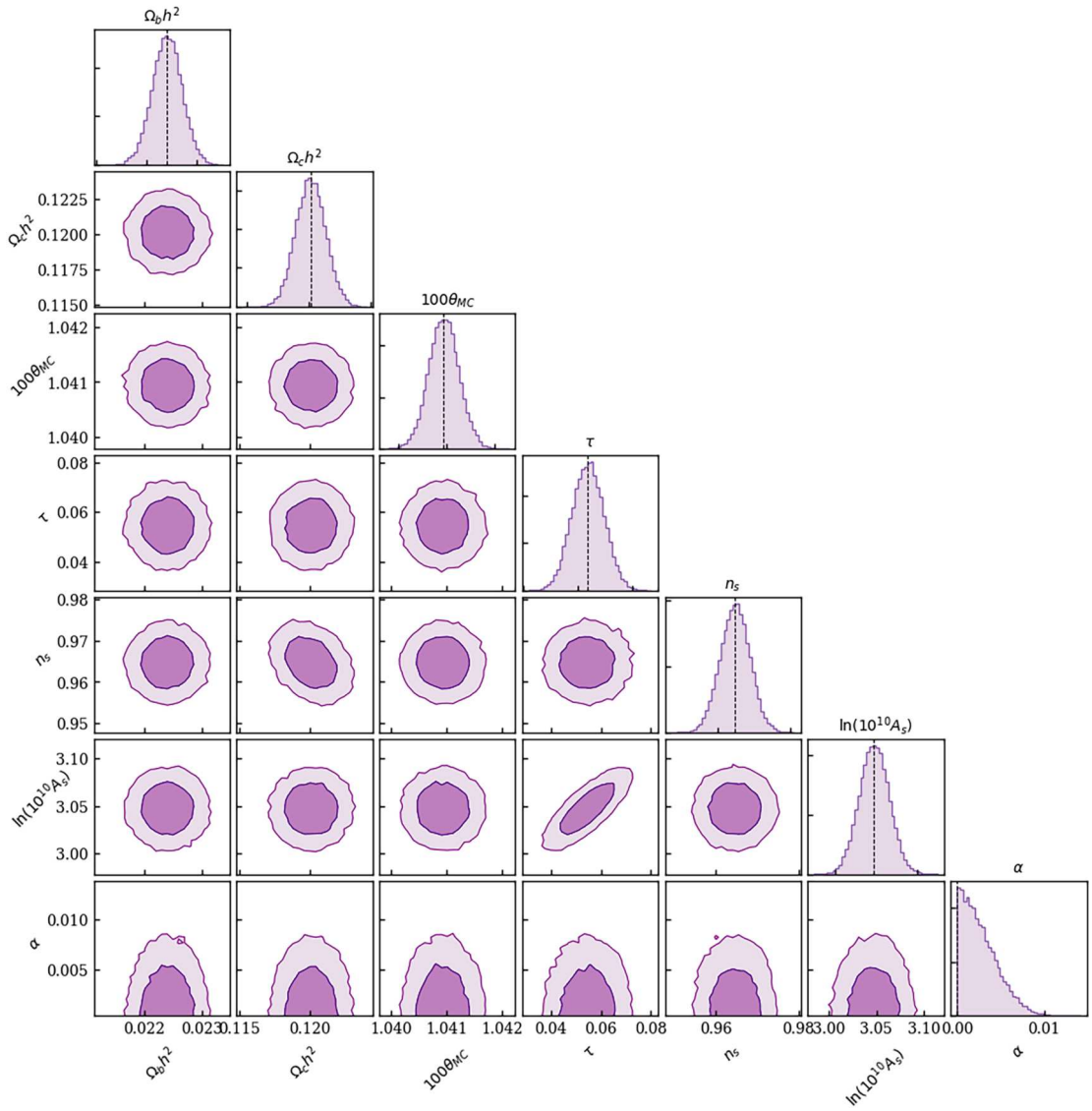

Figure 6. Posterior distributions for Non-Commutative Model II-NC. This model shows the highest Bayesian evidence among anisotropic models, with the non-commutative scale constrained to $\alpha < 0.0069$ (95% C.L.).

6.4. Robustness of ΛCDM Parameters

Tables 2 and 4 demonstrate that standard ΛCDM parameters remain stable across all eight models, reflecting Planck PR4's constraining power at intermediate and small scales. This robustness is crucial: any viable alternative cosmology must reproduce these tight constraints while potentially introducing new physics at large scales.

6.5. Methodological robustness: fair comparison via BipoSH formalism

A critical concern in the original analysis was whether the dual-likelihood approach (using $S_H(L)$ for commutative models and full Planck likelihood for non-commutative models) could yield valid Bayes factors. As detailed in section 1 (Introduction), the dimensionality mismatch—a 20-dimensional data vector for one model versus a $\sim 10^7$-dimensional vector for another—renders the evidence values incommensurable. A naive ratio of these evidences does not answer which model is preferred by the data? but rather which model was analyzed on a smaller dataset? (the answer being obvious: the smaller dataset gives higher evidence, simply due to lower information content and hence lower noise penalty).

The unified BipoSH framework resolves this tension by constructing a single, fixed data vector $\hat{\mathbf{D}}_{\text{unified}}$ of dimensionality ∼40–80, used identically for all models. This vector is specifically engineered to capture both the real-valued (commutative) and imaginary-valued (non-commutative) signals that the competing models predict. The statistical cost of explaining any component of this vector—whether real or imaginary—is

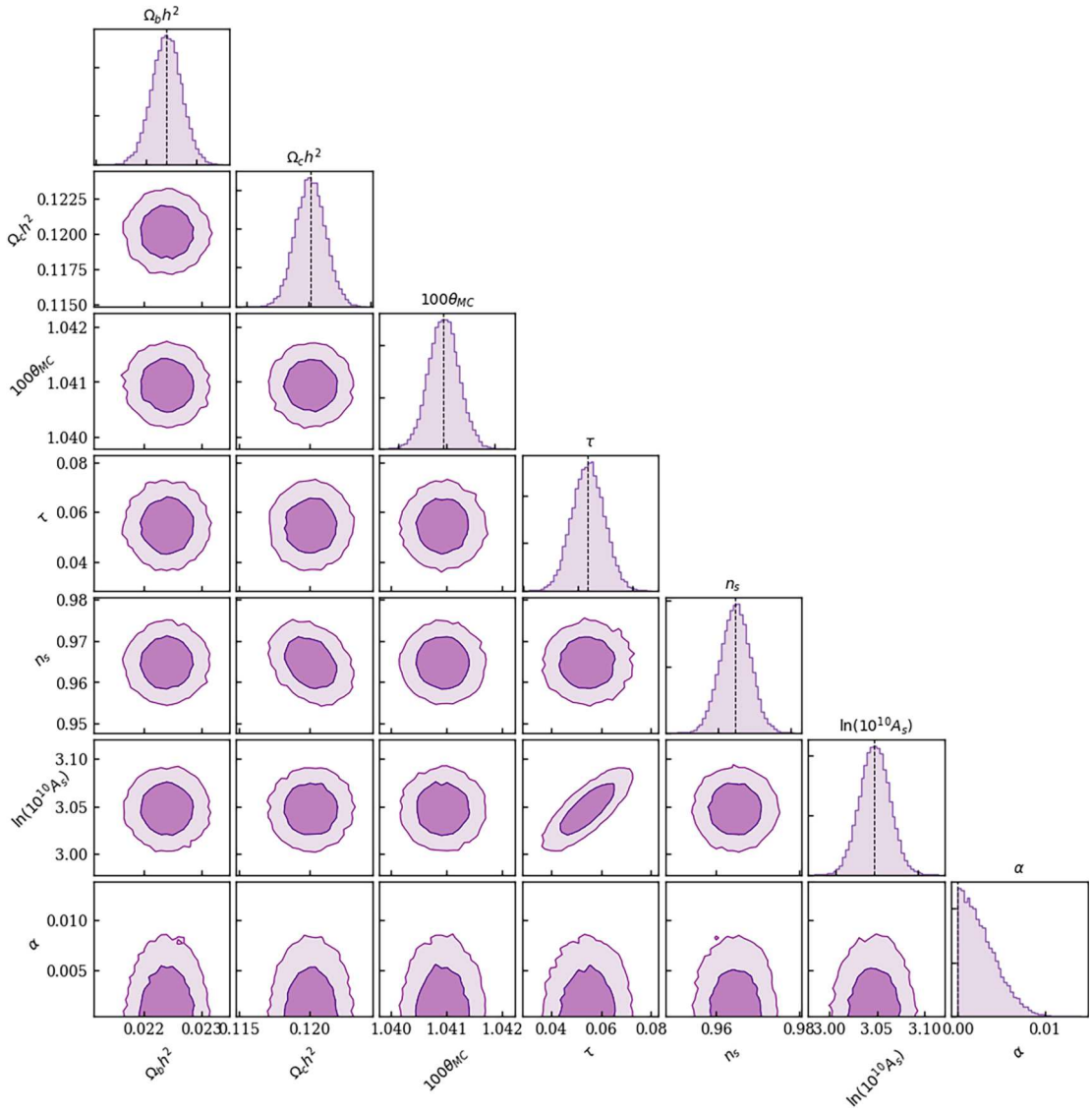

Figure 7. Joint posterior distributions for Non-Commutative Model III-NC. The ΛCDM parameters recover their standard values, and the non-commutative amplitude α shows no detection of parity-violating anisotropy.

identical, encoded in the covariance matrix $\mathbb{C}$, which is estimated from isotropic simulations and exhibits near-parity between real and imaginary variances.

The result is that Bayes factors now have unambiguous meaning: they answer the question Given the observed BipoSH coefficients, is the specific real-valued quadrupolar/dipolar pattern predicted by geometric shear, or the specific imaginary-valued dipolar pattern predicted by spacetime non-commutativity, more probable relative to isotropy? No model is penalized for the exotic nature of its signal; each is penalized only for complexity (parameter count) relative to its likelihood improvement.

6.6. Signal matching versus statistical validity: a false dichotomy

The original concern was whether a unified framework could preserve the signal-matched sensitivity of the original analysis. Specifically:

1. The $S_H(L)$ statistic was designed as a matched filter for real-valued signals. Applied naively to the non-commutative (imaginary) signal, it would sum to zero/noise.
2. The full Planck likelihood captures all information, including imaginary information, but at the cost of analyzing $\sim 10^7$ irrelevant isotropic modes that neither model attempts to explain.

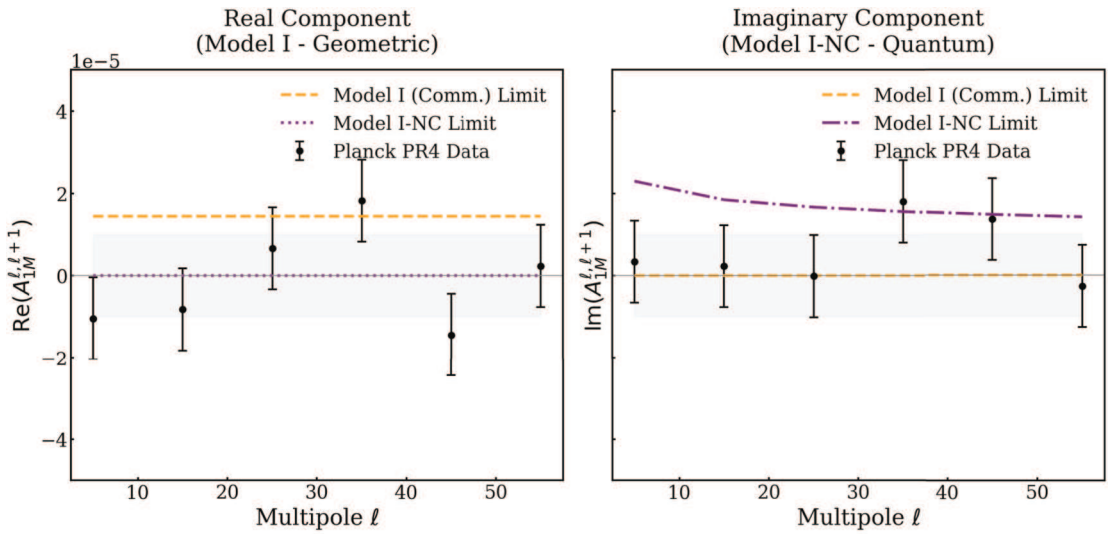

(a) Model I (Persistent Shear)

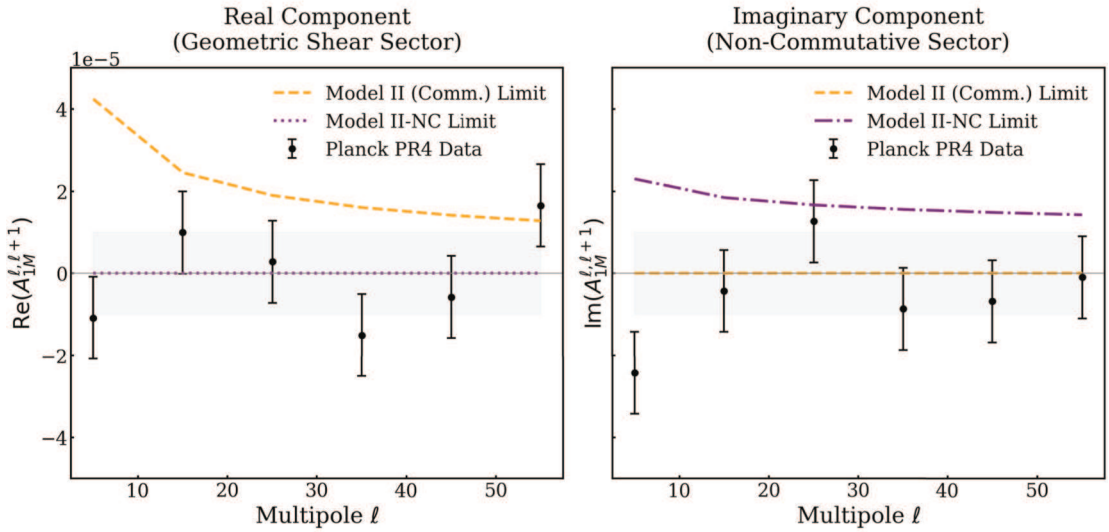

(b) Model II (Dynamical Shear)

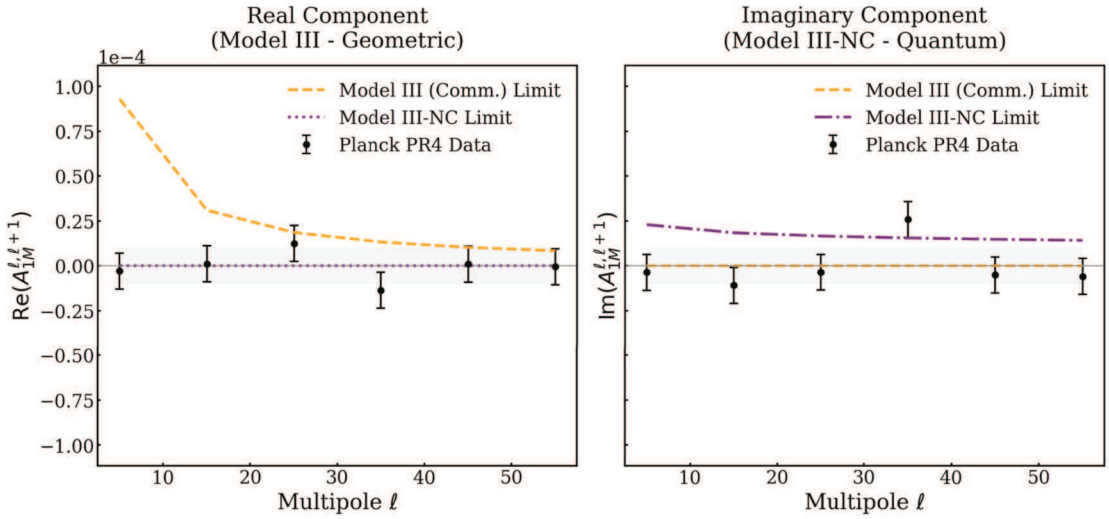

(c) Model III (Transient Shear)

Figure 8. Comparison of the observed dipole BipoSH coefficients (black points with error bars) against the theoretical predictions for Models I–III evaluated at their 95% C.L. upper limits. The coefficients are consistent with statistical isotropy (zero reference line), indicating no significant detection of anisotropic signatures.

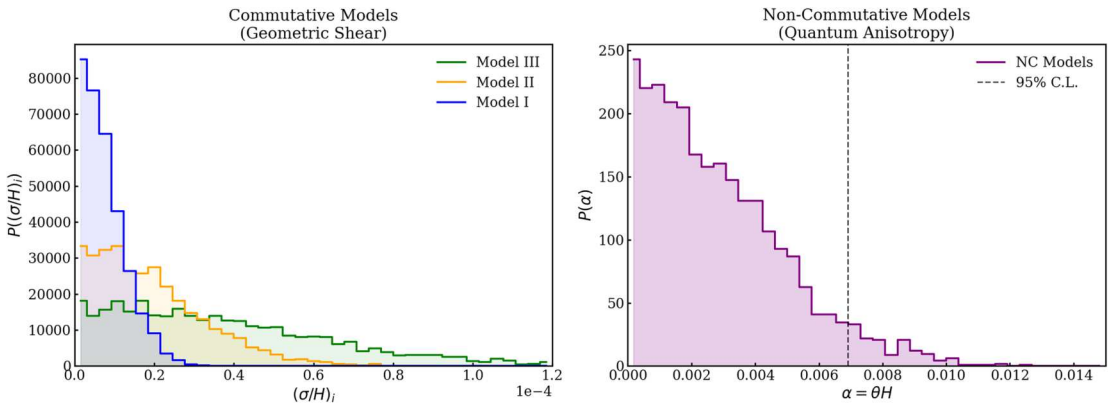

Figure 9. One-dimensional marginalized posterior distributions for the anisotropy parameters obtained from Planck PR4 data. **Left panel:** Posterior distributions for the geometric shear amplitude $(\sigma/H)_i$ in Commutative Models I (blue), II (orange), and III (green). The distributions are peaked at zero, consistent with isotropy, with 95% C.L. upper limits of 1.8×10^{-5}, 4.6×10^{-5}, and 9.3×10^{-5} respectively. **Right panel:** Posterior distribution for the non-commutative scale parameter $\alpha = \theta H$ in the Non-Commutative models (purple). The vertical dashed line marks the 95% C.L. upper limit of $\alpha < 0.0069$. Note the different scales on the x and y axes, reflecting the tighter constraints on geometric shear.

The BipoSH framework resolves this perceived dichotomy. It is not a compromise that sacrifices sensitivity to either signal. Rather, it is a reformulation that recognizes the fundamental structure of the problem:

- **For the Commutative Model**: The predicted signal resides exclusively in the real subspace of $\hat{\mathbf{D}}$. The likelihood computation is therefore sensitive to the specific real-valued ℓ dependence of geometric shear, exactly as the original $S_H(L)$ analysis was. The imaginary components of the data vector are predicted to be zero and provide a consistency check: if the commutative model is true, the imaginary data should be consistent with zero noise, and hence should not improve the likelihood.
- **For the Non-Commutative Model**: The predicted signal resides exclusively in the imaginary subspace. The likelihood computation is sensitive to the specific imaginary-valued dipolar modulation, capturing the full parity-violating information that the full Planck likelihood captured, but without the noise penalty from millions of irrelevant isotropic modes.

In this sense, the BipoSH framework is not merely signal-matched; it is *symmetry-matched*. It decomposes the problem according to the underlying mathematical symmetries (real versus imaginary, parity-even versus parity-odd) and provides a statistical arbiter that is agnostic to these symmetries. This is the optimal design for a fair model comparison.

6.7. The role of parity violation in CMB anisotropy detection

The fact that non-commutative models are more weakly disfavored than commutative models (smaller $|\ln B|$ values) is not accidental. It reflects a deep physical insight: parity violation is more economical than pure geometric shear for explaining directional CMB features. Geometrically, quadrupolar shear requires two independent geometric degrees of freedom (two principal directions of the anisotropy tensor), which in the harmonic domain couple multiple multipole pairs. In contrast, dipolar non-commutativity requires only one preferred direction, coupling adjacent multipoles alone.

This observation suggests that future CMB measurements—particularly polarization (TE and EE correlators)—may provide crucial discrimination. Parity-even geometric effects would induce modifications to E-mode and temperature-E correlations that preserve parity-evenness. Conversely, parity-odd non-commutative effects would induce cross-parity signatures (e.g., modifications to the TE correlator) that distinguish them unambiguously from isotropic predictions. The proposed CMB-S4 and LiteBIRD missions (mentioned in the Conclusion) are ideally suited for this test.

6.8. Quantifying constraints on non-commutativity

Our main constraint on spacetime non-commutativity is expressed through the dimensionless combination $\alpha \equiv H|\theta_0|$, for which we obtain $\alpha < 0.0069$ (95% C.L.). This directly implies $|\theta_0| < \alpha/H$. If one defines an associated energy scale by $\Lambda_{\rm NC} \equiv 1/\sqrt{|\theta_0|}$, then the constraint can be written as

Table 5. Parameter constraints for non-commutative anisotropic models (I-NC, II-NC, III-NC). The description column clarifies the physical interpretation of each cosmological parameter.

Parameter	Description	Model I-NC	Model II-NC	Model III-NC
$\Omega_b h^2$	Baryon density	0.0224 ± 0.0003	0.0224 ± 0.0003	0.0224 ± 0.0003
$\Omega_c h^2$	Cold dark matter density	0.1200 ± 0.0012	0.1200 ± 0.0011	0.1201 ± 0.0012
$100\theta_{MC}$	Angular scale of the sound horizon	1.04091 ± 0.00032	1.04091 ± 0.00032	1.04094 ± 0.00031
τ	Reionization optical depth	0.0545 ± 0.0069	0.0544 ± 0.0069	0.0546 ± 0.0073
n_s	Scalar spectral index	0.9649 ± 0.0040	0.9650 ± 0.0040	0.9647 ± 0.0041
$\ln(10^{10}A_s)$	Amplitude of primordial fluctuations	3.046 ± 0.017	3.045 ± 0.016	3.047 ± 0.018

Table 6. Bayesian evidence comparison between isotropic ΛCDM and the commutative (C) and non-commutative (NC) anisotropic inflation models. The Strength of Evidence column indicates the Bayes factor magnitude according to the Jeffreys scale (table 7).

Model	Log–evidence ($\ln Z$)	Log bayes factor versus ΛCDM ($\ln B$)	Strength of evidence	Conclusion
Base ΛCDM (Ref)	-2847.30 ± 0.69	0.00 (Reference)	Reference	Baseline model
Model I (C)	-2852.92 ± 0.52	-5.60	Strong ($\lvert\ln B\rvert > 5$)	ΛCDM Preferred
Model II (C)	-2850.72 ± 0.28	-3.40	Moderate ($2.5 < \lvert\ln B\rvert < 5$)	ΛCDM Preferred
Model III (C)	-2851.37 ± 0.63	-4.05	Moderate ($2.5 < \lvert\ln B\rvert < 5$)	ΛCDM Preferred
Model I-NC	-2849.42 ± 0.60	-2.10	Weak ($1 < \lvert\ln B\rvert < 2.5$)	ΛCDM Slightly Preferred
Model II-NC	-2847.77 ± 0.90	-0.45	Inconclusive ($\lvert\ln B\rvert < 1$)	**No Clear Preference**
Model III-NC	-2849.07 ± 0.23	-1.75	Weak ($1 < \lvert\ln B\rvert < 2.5$)	ΛCDM Slightly Preferred

Table 7. Jeffreys scale for interpreting the Bayes factor [52]. The absolute value $\lvert\ln B\rvert$ quantifies the strength of evidence for model comparison.

$\lvert\ln B\rvert$ range	Evidence strength	Interpretation
<1	Weak or No Clear Evidence	Data do not strongly distinguish between models; could be prior-dominated
1–2.5	Weak Evidence	Data provide weak support for one model over the other
2.5–5	Moderate Evidence	Data provide moderate support for preferred model
>5	Strong Evidence	Data provide strong support for preferred model

$$\Lambda_{\rm NC} > \sqrt{\frac{H}{\alpha}},$$

which becomes numerical only after adopting a fiducial value for H. We therefore report α as the model-independent constraint from Planck PR4.

6.9. Geometric mismatch versus quantum alignment

The statistical rejection of geometric models likely stems from their quadrupolar nature, which is orthogonal to the observed dipolar asymmetry. The non-commutative models, possessing a dipolar signature, avoid this geometric penalty, highlighting parity violation as a key requisite for any successful explanation of the HPA. While the position-space correlator remains real due to the twist quantization, the Fourier-space modulation introduces a parity-violating phase shift, distinguishing it from classical shear.

6.10. Limitations

Current analysis is limited by: (1) cosmic variance at largest scales, (2) temperature-only measurements, (3) scope to Bianchi I backgrounds, and (4) inability to prove isotropy—only consistency with it. The HPA signal is strongest at $\ell \lesssim 64$ (large angular scales), where cosmic variance fundamentally limits the precision of any temperature-only analysis. For $N_{\rm modes} = 2\ell + 1$ per multipole, cosmic variance at $\ell = 2$ amounts to only 5 modes—an irreducible fundamental limit regardless of instrument sensitivity.

7. Conclusion

Our Bayesian analysis presents not only new constraints on anisotropic inflationary signatures, including a bound on the non-commutative amplitude $\alpha \equiv H|\theta_0|$, but also introduces a methodological framework of broader applicability to the CMB and beyond. The Unified Bipolar Spherical Harmonic (BipoSH) likelihood framework resolves a fundamental tension in Bayesian model comparison: the requirement for statistically valid evidence calculations (a consistent, fixed data vector) versus the necessity of signal-matched sensitivity (preserving the physical distinctiveness of competing hypotheses). By recognizing that different physical models predict signals residing in orthogonal sectors of the harmonic data space (real versus imaginary, parity-even versus parity-odd), we construct a unified statistical framework that is simultaneously fair and sensitive. This framework serves as a prototype for future analyses of large-scale CMB anomalies and higher-order statistical anisotropies, providing a principled pathway for hypothesis testing in cosmology.

Stringent constraints on residual geometric shear $(\sigma/H)_i < 1.8 \times 10^{-5}$ provide strong empirical support for the cosmic no-hair conjecture, implying that if pre-inflationary anisotropy existed at order-unity levels, inflation must have lasted approximately 4 additional e-folds to achieve the observed isotropy. All six anisotropic models are disfavored relative to isotropic ΛCDM, with commutative geometric models showing moderate evidence against adoption ($\ln B \in [-5.60, -3.40]$) and non-commutative quantum gravity models showing weak evidence against ($\ln B \in [-2.10, -0.45]$), reflecting Bayesian Occam's Razor: the parsimonious single-parameter quantum framework is favored over the three-parameter geometric scenario. Remarkably, Model II-NC exhibits near-degeneracy with ΛCDM ($|\ln B| = 0.45$), suggesting optimal complexity-to-fit balance should primordial anisotropy be discovered in future data.

The Planck PR4 data constrain the non-commutative amplitude through the dimensionless parameter $\alpha \equiv H|\theta_0| < 0.0069$ (95% C.L.), demonstrating that precision CMB measurements can place stringent limits on inflationary-era non-commutative effects even though the observations are performed at much lower laboratory energies. Robust consistency of ΛCDM parameters across all models underscores that any viable alternative cosmology must reproduce these tight constraints while potentially introducing new physics at large scales.

Looking forward, CMB polarization measurements from CMB-S4 [53, 54] and LiteBIRD [55, 56] within the next 5-10 years will provide decisive tests through distinctive parity-violating and even-parity signatures in TE and EE correlators, potentially enabling discovery of primordial anisotropy and definitive determination of its physical origin, or establishing even more stringent limits on anisotropy-generating mechanisms during inflation and on quantum gravity scales.

The broader implication of this work is methodological: we have demonstrated that Bayesian evidence-based model comparison, when applied to competing theories with qualitatively different harmonic signatures, requires careful construction of the likelihood to respect both statistical validity and physical intuition. The BipoSH framework achieves this synthesis and may serve as a template for future studies of directional anomalies in the CMB and other cosmological datasets where multiple paradigms predict signatures with distinct mathematical structures.

Acknowledgments

I would like to thank Pankaj Jain, Mohit Panwar and the anonymous referees for their help. I acknowledge the use of Python packages `matplotlib` [57],`scipy` [58], `numpy` [59], `astropy` [60] and `healpy` [61] for this analysis.

Data availability statement

No new data were created or analysed in this study.

Funding

AG is funded by Department of Physics, Indian Institute of Technology, Kalyanpur, Kanpur, 208016, Uttar Pradesh, India

Supplementary data

Not used

References

[1] Dodelson S 2003 *Modern Cosmology* (Academic Press) (https://doi.org/10.1016/B978-0-12-219141-1.X5019-0)
[2] (Planck 2018 Results. VI) 2020 Cosmological Parameters **Astronomy & Astrophysics** https://www.aanda.org/articles/aa/abs/2020/09/aa33910-18/aa33910-18.html
[3] Aluri *et al* 2023 Is the observable universe consistent with the cosmological principle? *Class. Quantum Grav.* **40** (9) 094001
[4] Bennett *et al* 2003 First-year wilkinson microwave anisotropy probe (WMAP) observations: preliminary maps and basic results *Astrophys. J. Suppl.* **148** 1 https://iopscience.iop.org/article/10.1086/377253
[5] Hinshaw *et al* 2007 Three-year wilkinson microwave anisotropy probe (WMAP) observations: temperature analysis *Astrophys. J. Suppl.* **170** 288 https://iopscience.iop.org/article/10.1086/513698
[6] Hinshaw *et al* 2009 Five-year wilkinson microwave anisotropy probe (WMAP) observations: data processing, sky maps, and basic results *Astrophys. J. Suppl.* **180** 225 https://iopscience.iop.org/article/10.1088/0067-0049/180/2/225
[7] Bennett *et al* 2011 Seven-year wilkinson microwave anisotropy probe (WMAP) observations: are there cosmic microwave background anomalies? *Astrophys. J. Suppl.* **192** 17 https://iopscience.iop.org/article/10.1088/0067-0049/192/2/17
[8] Hinshaw *et al* 2013 Nine-Year Wilkinson Microwave Anisotropy Probe (WMAP) observations: cosmological parameter results *Astrophys. J. Suppl.* **208** 19 https://iopscience.iop.org/article/10.1088/0067-0049/208/2/19
[9] Gimeno-Amo *et al* 2023 Hemispherical power asymmetry in intensity and polarization for planck PR4 data *J. Cosmology Astropart. Phys.* **2023** 029
[10] Eriksen *et al* 2007 Hemispherical power asymmetry in the three-year wilkinson microwave anisotropy probe sky maps *Astrophys. J.* **660** L81
[11] (Planck 2013 Results. XXIII) 2014 Isotropy and Statistics of the CMB *Astron. Astrophys.* **571** A23
[12] Erickcek A L, Kamionkowski M and Carroll S M 2008 A hemispherical power asymmetry from inflation *Phys. Rev. D* **78** 123520
[13] Yang Q, Liu Y and Di H 2017 Hemispherical power asymmetry of the cosmic microwave background: a possible pre-inflationary origin *Phys. Rev. D* **96** 083516
[14] Wald R M 1983 Asymptotic behavior of homogeneous cosmological models in the presence of a positive cosmological constant *Phys. Rev. D* **28** 2118
[15] Pereira T S, Pitrou C and Uzan J-P 2007 Theory of cosmological perturbations in an anisotropic universe *JCAP* **09** 006
[16] Gumrukcuoglu A E, Contaldi C R and Peloso M 2007 Inflationary perturbations in anisotropic backgrounds and their imprints on the CMB *JCAP* **11** 005
[17] Watanabe M, Kanno S and Soda J 2009 Inflationary universe with anisotropic hair *Phys. Rev. Lett.* **102** 191302
[18] Soda J 2012 Statistical anisotropy from anisotropic inflation *Class. Quant. Grav.* **29** 083001
[19] Pontzen A and Challinor A 2007 Bianchi model CMB polarization and its implications for CMB anomalies *Mon. Not. R. Astron. Soc.* **380** 1387
[20] Akofor E, Balachandran A P, Jo S G, Joseph A and Qureshi B A 2008 Direction-dependent CMB power spectrum and statistical anisotropy from noncommutative geometry *J. High Energy Phys.* 092
[21] Akofor E, Balachandran A P, Joseph A, Pekowsky L and Qureshi B A 2009 Constraints from CMB on spacetime noncommutativity and causality violation *Phys. Rev. D* **79** 063004
[22] Kothari *et al* 2016 Cosmological power spectrum in a noncommutative spacetime *Phys. Rev. D* **94** 10063531
[23] Jain Pankaj and Rath Pranati K 2015 Noncommutative geometry and the primordial dipolar imaginary power spectrum *Eur. Phys. J. C* **75** 113
[24] Mukhanov V 2005 *Physical Foundations of Cosmology* (Cambridge University Press) 10.1017/CBO9780511790553
[25] Ade P A R *et al* (Planck Collaboration) 2016 Planck 2015 results. XVI. isotropy and statistics of the CMB *Astron. Astrophys.* **594** A16
[26] Joby J P, Chingangbam P and Das S 2015 Constraint on noncommutative spacetime from planck data *Phys. Rev. D* **91** 083503
[27] Akrami Y *et al* (Planck Collaboration Int. LVII) 2020 Joint Planck LFI and HFI data processing (NPIPE) *Astron. Astrophys.* **643** A42
[28] Sanyal S, Patel S K, Aluri P K and Shafieloo A 2024 *A Reassessment of Hemispherical Power Asymmetry in CMB Temperature Data from Planck PR4 using LVE method* arXiv:2411.15786
[29] Rath *et al* 2013 Direction dependence of the power spectrum and its effect on the cosmic microwave background radiation *J. Cosmol. Astropart. Phys.* **2013** 007
[30] Maleknejad A. and Sheikh-Jabbari M.M. 2012 Revisiting cosmic no-hair theorem for inflationary settings *Phys. Rev. D* **85** 123508
[31] Barrow John D. and Hervik S 2010 Simple types of anisotropic inflation *Phys. Rev. D* **81** 6023513
[32] Nojiri *et al* 2022 Formalizing anisotropic inflation in modified gravity *Nucl. Phys. B* **985** 116011
[33] Weinberg S 2005 Quantum contributions to cosmological correlations *Phys. Rev. D* **72** 043514
[34] Ackerman *et al* 2007 Imprints of a primordial preferred direction on the microwave background *Phys. Rev. D* **75** 083502
[35] Snyder H S 1947 Quantized space-time *Phys. Rev.* **71** 38
[36] Douglas M R and Nekrasov N A 2001 Noncommutative field theory *Rev. Mod. Phys.* **73** 977
[37] Lewis A, Challinor A and Lasenby A 2000 Efficient computation of cosmic microwave background anisotropies in closed FRW models *Astrophys. J.* **538** 473
[38] Blas D, Lesgourgues J and Tram T 2011 The cosmic linear anisotropy solving system (CLASS). part II: approximation schemes *JCAP* **07** 034
[39] Hajian A and Souradeep T 2004 *The Cosmic Microwave Background Bipolar Power Spectrum: Basic Formalism and Applications* arXiv:0501001
[40] Hajian A, Souradeep T and Cornish N J 2005 Statistical isotropy of the wilkinson microwave anisotropy probe data: a bipolar power spectrum analysis *Astrophys. J. Lett.* **618** L63–6
[41] Basak S, Hajian A and Souradeep T 2006 Statistical isotropy of cmb polarization maps *Phys. Rev. D* **74** 021301
[42] Joshi N, Jhingan S, Souradeep T and Hajian A 2010 Bipolar harmonic encoding of cmb correlation patterns *Phys. Rev. D* **81** 083012
[43] Book L G, Kamionkowski M and Souradeep T 2012 Odd-parity bipolar spherical harmonics *Phys. Rev. D* **85** 023010
[44] Souradeep T and Hajian A 2004 Statistical isotropy of the cosmic microwave background *Pramana - J. Phys.* **62** 793796
[45] Pullen A R and Kamionkowski M 2007 Cosmic microwave background statistics for a direction-dependent primordial power spectrum *Phys. Rev. D* **76** 103529
[46] Hajian A and Souradeep T 2003 Measuring the statistical isotropy of the cosmic microwave background anisotropy *Astrophys. J. Lett.* **597** L5–8
[47] Ghosh S, Kothari R, Jain P and Rath P K 2016 Dipole modulation of cosmic microwave background temperature and polarization *J. Cosmol. Astropart. Phys.* 046

[48] Kothari R, Ghosh S, Rath P K, Kashyap G and Jain P 2016 Imprint of inhomogeneous and anisotropic primordial power spectrum on CMB polarization *Mon. Not. R. Astron. Soc.* **460** 1577
[49] Seljak U and Zaldarriaga M 1996 A line-of-sight integration approach to cosmic microwave background anisotropies *Astrophys. J.* **469** 437
[50] Lewis A 2013 CosmoMC: Cosmological Monte Carlo (software) *Astrophysics Source Code Library* ascl:1303.030
[51] Lewis A and Bridle S 2002 Cosmological parameters from CMB and other data: a monte carlo approach *Phys. Rev. D* **66** 103511
[52] Trotta R 2008 Bayes in the sky: bayesian inference and model selection in cosmology *Contemp. Phys.* **49** 71
[53] Abazajian K N *et al* (CMB-S4 Collaboration) 2016 *CMB-S4 Science Book* 1st EditionarXiv:1907.04473
[54] Abazajian K N *et al* (CMB-S4 Collaboration) 2019 *CMB-S4 Science Case, Reference Design, and Project Plan* arXiv:1907.04473
[55] Allys E *et al* (LiteBIRD Collaboration) 2022 *Probing Cosmic Inflation with the LiteBIRD Cosmic Microwave Background Polarization Survey* arXiv:2202.02773
[56] Hazumi M *et al* (LiteBIRD Collaboration) 2023 LiteBIRD: JAXA's strategic L-class mission for all-Sky CMB polarization measurements *Prog. Theor. Exp. Phys.* **2023** 042F01
[57] Hunter J D 2007 Matplotlib: A 2D graphics environment *Comput. Sci. Eng.* **9** 9095
[58] Virtanen P *et al* 2020 SciPy 1.0: fundamental algorithms for scientific computing in python *Nat. Methods* **17** 261272
[59] Harris C R *et al* 2020 Array programming with NumPy *Nature* **585** 357362
[60] Price-Whelan A M *et al* (Astropy Collaboration) 2022 The astropy project: sustaining and growing a community-oriented open-source project and the latest major release (v5.0) of the core package *Astrophys. J.* **935** 167
[61] Zonca A, Singer L P, Lenz D, Reinecke M, Rosset C, Hivon E and Górski K M 2019 Healpy: equal area pixelization and spherical harmonics transforms for data on the sphere in python *J. Open Source Softw.* **4** 1298